REVIEW ARTICLE

Rydberg atoms

Rep. Prog. Phys. **51** (1988) 143–188. Printed in the UK

Rydberg atoms

T F Gallagher

Department of Physics, University of Virginia, Charlottesville, VA 22901, USA

Abstract

Recent investigations of Rydberg atoms are described in an effort to give a picture of their properties, many of which can be understood from the behaviour of the Coulomb radial functions. Thus we begin by a discussion of Coulomb wavefunctions, and progress quickly to a description of the energy level structure. The behaviour of Rydberg atoms in electric fields is discussed to provide an understanding of the phenomenon and to show how electric field ionisation may be used as a tool in a wide variety of experiments. The unique opportunities to study the interaction with blackbody radiation and the vacuum fluctuations are then discussed. A survey of the broad range of Rydberg atom collisions, with ground-state atoms and molecules, charged particles and other Rydberg atoms, is presented to show the different physical interactions responsible. This is followed by a brief summary of the study of autoionising Rydberg states, a stepping stone toward the elusive 'double Rydberg' atom. Finally typical experimental procedures are described.

This review was received in April 1987.

0034-4885/88/020143+46$09.00

Contents

1. Introduction

The first explorations of the unique properties of Rydberg atoms were begun about fifty years ago by Amaldi and Segre (1934) who investigated the pressure shifts and broadening of Rydberg levels of Na and K by rare gases. It had been thought that the presence of the rare gas atoms inside the large orbit of a Rydberg atom would be similar to the presence of a dielectric and would lead to a red shift of all the lines. However, Amaldi and Segre discovered not only red but also blue shifts, in direct contradiction to the dielectric model. Fermi (1934) pointed out that the dielectric, or polarisation, effect was but one of the two effects that needed to be considered. The other, the short-range interaction of the low-energy electron with the rare gas atom, had not been included. When this larger effect is properly taken into account, the observations agree with the predictions almost exactly. This was probably the first example of using Rydberg atoms to study low-energy electron scattering.

Somewhat later, Jenkins and Segre (1939) recognised that Rydberg atoms with their enormous orbital radii presented the best available opportunity for the observation of atomic diamagnetism, which depends on the area of the Rydberg electron's orbit, and they observed the absorption spectrum of K in the 10 kG field of the Berkeley cyclotron magnet. While their results have been overshadowed by more recent experiments at higher fields, their measurements show in a very clear fashion the quadratic energy shifts and the mixing of the l states produced by the diamagnetic interaction.

The interest in Rydberg atoms lay dormant until they reappeared in several astrophysical circumstances. The radio recombination lines between Rydberg states of several light atoms have been observed from interstellar regions of low density where the Rydberg atoms can live long enough to decay radiatively (Höglund and Metzger 1965). The observed lines are the $n \rightarrow n-1$ transitions which originate from Rydberg states produced by direct radiative recombination of low-energy electrons with ions. At the other end of the temperature scale, in hot astrophysical and laboratory plasmas, hot electrons can most efficiently recombine with ions by being captured into autoionising Rydberg states which subsequently decay radiatively to bound Rydberg states, a process termed dielectronic recombination (Dubau and Volonté 1980).

The primary motivation for the study of Rydberg atoms today is, not so differently from what it was fifty years ago, to take advantage of the unique opportunities afforded by their exaggerated properties. Consider an example. To expose a ground-state atom to an electric field comparable to the Coulomb field experienced by the valence electron requires a field of $10^9\ \mathrm{V\,cm^{-1}}$ or, in the case of a radiation field, an intensity of $10^{14}\ \mathrm{W\,cm^{-2}}$, a level which can only be reached by the highest-power pulsed lasers when focused to a diffraction-limited spot. On the other hand, in a Rydberg atom of principal quantum number $n = 20$ the electron at its most probable orbital radius is in a Coulomb field of $\sim 10^3\ \mathrm{V\,cm^{-1}}$. It is straightforward to produce fields of this magnitude in a controlled fashion, opening the door to more quantitative studies of atoms in strong radiation fields than are possible using ground-state atoms and intense lasers.

A second relatively unique aspect of Rydberg states is their regularity. They provide an opportunity for systematic and self-consistent studies by virtue of the n dependence of virtually all atomic properties. Stated another way, every observed phenomenon

depends upon some atomic property and must display a regular n dependence. This provides an easily applied check for the accuracy or consistency of many measurements. On the other hand, the systematic variation of properties with n offers some new opportunities which do not exist elsewhere. A good example of this is the use of the $1/n^3$ scaling of energy level separations to observe resonances in collisional energy transfer. For example, a 2000 cm^{-1} vibrational energy spacing matches the hydrogen $n=9\rightarrow 8$ transition, but no other, so one might hope to see an anomalously large quenching cross section for the $n=9$ level, with the increase over the quenching cross sections of $n=8$ and 10 being due to the resonant $n=9\rightarrow 8$ collisional transition. In fact, several examples of resonant energy transfer have been observed, including electronic to vibrational, rotational and electronic energy transfer (Smith *et al* 1978, Gallagher *et al* 1980, Safinya *et al* 1981).

A goal in recent work has been to reach an understanding of doubly excited Rydberg states in which each of two electrons is excited to a Rydberg state. There has been a substantial amount of theoretical work devoted to this problem, beginning with that of Percival (1977) who considered what he termed 'planetary atoms', i.e. atoms in which one electron is in a substantially larger orbit than the other. More recent theoretical work has focused on highly correlated systems in which both electrons have roughly equivalent excitations. This work, based on a hyperspherical coordinate approach (Lin 1983, 1984) and group theory approaches (Herrick and Kellman 1980, Herrick *et al* 1980), has led to a variety of provocative predictions. Unfortunately, experimental progress on this problem has been much slower. Although it has been possible to make autoionising Rydberg states, even converging to highly excited states of Ba^+, it has not yet been possible to observe states which exhibit a large degree of correlation of the two electrons. To date the observations can all be understood in terms of one electron added to an excited positive ion core.

The goal of this review is to convey the basic notions required to appreciate much of the recent research on Rydberg atoms. With this in mind only selected topics which have broad impact are discussed. Electric fields are discussed since an understanding of electric field ionisation is critical to its use in other experiments. On the other hand, magnetic fields are not discussed, in spite of very interesting work along these lines. It is the hope of the author that this review will serve to convey the flavour of recent research.

2. Structure and properties

In discussing the structure and properties of atomic Rydberg states it is convenient to introduce atomic units which are defined so that all the parameters for the ground state of H have magnitude one. The atomic units most useful for our purposes are given in table 1.

Using atomic units we may write the time-independent Schrödinger equation for a hydrogen atom as

$$(-\tfrac{1}{2}\nabla^2 - 1/r)\psi = W\psi \tag{2.1}$$

where r is the distance of the electron from the proton and W is its energy. The purely radial $1/r$ Coulomb potential allows the separation into angular and radial equations with the result that the solutions are given by the product

$$\psi(nlm) = R_{nl}(r)\, Y_{lm}(\theta, \phi). \tag{2.2}$$

Table 1. Atomic units.

Quantity	Atomic unit	Definition
Charge	electron charge e	1.6×10^{-19} C
Energy	twice the ionisation potential of hydrogen	27.2 eV
Length	radius of a_0, the first Bohr orbit	0.529 Å
Velocity	velocity of the first Bohr orbit	2.19×10^{8} cm s^{-1}
Electric field	field at the first Bohr orbit	5.14×10^{9} V cm^{-1}

The position of the electron relative to the proton is given in the spherical coordinates r, θ and ϕ, where θ is the polar angle relative to the quantisation axis and ϕ is the azimuthal angle. Here n, l and m are the radial, orbital angular momentum and azimuthal angular momentum quantum numbers. The angular equation yields the normalised spherical harmonics $Y_{lm}(\theta, \phi)$ as solutions. The radial equation is given by (Bethe and Salpeter 1957)

$$\frac{d^2R}{dr^2}+\frac{2}{r}\frac{dR}{dr}+2WR+\frac{2R}{r}=\frac{l(l+1)R}{r^2} \tag{2.3}$$

which has two physically interesting solutions:

$$R(r)=f(l, r, W)/r \tag{2.4a}$$

and

$$R(r)=g(l, r, W)/r. \tag{2.4b}$$

The f and g functions are commonly termed the regular and irregular Coulomb functions (Fano 1970, Seaton 1983). In the classically allowed region the f and g functions are oscillatory functions with a phase difference of 90°. As $r\to0$

$$f(l, W, r)\propto r^{l+1} \tag{2.5a}$$

and

$$g(l, W, r)\propto r^{-l}. \tag{2.5b}$$

For $W<0$ the effective quantum number ν, defined by $W=-1/2\nu^2$ is useful. For $r\to\infty$ the f and g functions may be expressed in terms of increasing and decreasing exponential functions $u(l, \nu, r)$ and $v(l, \nu, r)$. As $r\to\infty$ $u\to\infty$ and $v\to0$, and f and g are given by

$$\begin{aligned} f &\to u(\nu, r)\sin(\pi\nu)-v(\nu, r)\exp(i\pi\nu) \\ g &\to -u(\nu, r)\cos(\pi\nu)+v(\nu, r)\exp[i\pi(\nu+\tfrac{1}{2})]. \end{aligned} \tag{2.6}$$

Applying the boundary conditions for the hydrogen atom, i.e. that ψ be finite as $r\to0$ and that $\psi\to0$ as $r\to\infty$, we can see from (2.5) that only the f functions are allowed due to the $r=0$ boundary condition. Applying the $r=\infty$ boundary condition to the f function is equivalent to requiring that $\sin(2\pi\nu)$ be zero or that ν be an integer. Thus for the hydrogen atom we recover the familiar condition that the allowed energies are given by

$$W=-1/2n^2 \tag{2.7}$$

where n is an integer.

While the asymptotic behaviour plays a key role in the boundary conditions, we can get further insight into the characteristics of the wavefunction by examining the WKB wavefunctions. For the region $(l+\frac{1}{2})^2 \ll r \ll n^2$, where the kinetic energy of the electron is independent of n, the WKB solution is given by (Bethe and Salpeter 1957):

$$R_{nl}(r) = Nr^{-3/4}\cos[\sqrt{8r} - 2(l+1)] \tag{2.8}$$

N being a normalisation constant. Note that $R_{nl}(r)$ is an oscillating function of spatial frequency which decreases as $1/\sqrt{r}$, corresponding to the change in momentum of the Rydberg electron in the $1/r$ Coulomb potential, and of amplitude which varies as $r^{+3/4}$. The other useful aspect of the WKB wavefunction is that it enables us to determine the normalisation constant of the radial wavefunction. For bound states $R_{nl}(r)$ must satisfy the normalisation condition

$$\int_0^\infty r^2 R_{nl}(r) R_{nl}^*(r)\,\mathrm{d}r = 1. \tag{2.9}$$

Approximating $\cos^2[\sqrt{8r} - 2(l+1)]$ by its average value, $\frac{1}{2}$, and integrating over the classically allowed region $0 < r, 2n^2$, we find $N = (3/4\sqrt{2n^3})^{1/2}$. Thus the overall amplitude of the radial wavefunction scales as $n^{-3/2}$. As we shall see shortly the normalisation enters into a variety of properties. From our discussion of the WKB wavefunction it is apparent that at small r, where the kinetic energy of the electron is large, the wavefunctions of all n of the same l differ only by their $n^{-3/2}$ normalisation constants.

The previous discussion of hydrogen may be extended to non-hydrogenic atoms using quantum defect theory (Seaton 1983). To do this we first recall the difference between a sodium atom and a hydrogen atom, i.e. the presence of the finite-sized ion core of the Na atom. Far from the Na^+ core the potential experienced by the valence electron is indistinguishable from that due to a proton. However, at small orbital radii the outer electron can both penetrate and polarise the ten electrons of the Na^+ core. As a result of this, at small orbital radii the Na potential is lower than the Coulomb potential. In figure 1 we show in a very schematic way the Coulomb potential and the potential seen by the Rydberg electron in the Na atom.

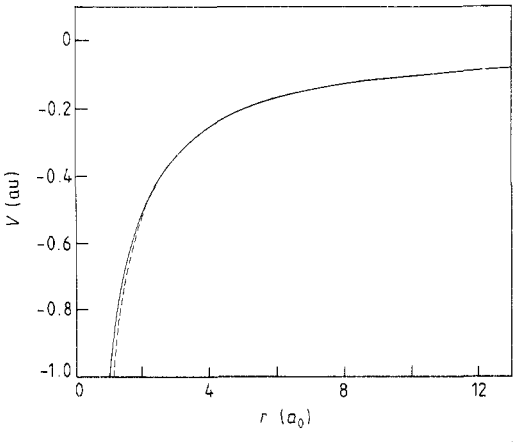

Figure 1. Schematic Coulomb potential of hydrogen (full curve) and the effective one-electron potential of Na (broken curve) which is different from the Coulomb potential only at small r.

The effect of the lower potential seen by the electron in Na is to increase the spatial frequency of the radial oscillations, pulling all the nodes of the radial wavefunction closer to the origin. For $r > r_0$, the radius of the Na^+ core, the Na potential is very nearly equal to the Coulomb potential. Thus in this region the wavefunction is simply shifted in phase from the hydrogen wavefunction. The magnitude of the radial phase shift is simply the difference in momentum of an electron of energy W in Na and H integrated from r to r_0. Explicitly, the phase shift relative to H can be written as

$$\tau = \int_0^{r_0} [(W - V_{Na}(r))^{1/2} - (W + 1/r)^{1/2}]\, dr. \tag{2.10}$$

The terms in the first and second parentheses are the kinetic energies of the electron in Na and H respectively. If we replace $V_{Na}(r)$ by $-1/r - V_d(r)$, where V_d is the difference between the Na and H potentials, and take advantage of the fact that for $r < r_0$ the kinetic energy is large so that $1/r \gg W$ and $V_d(r)$, we can expand (2.10). Keeping the first-order terms in the expansion leads to

$$\tau = \int_0^{r_0} \tfrac{1}{2} V_d(r) r^{1/2}\, dr. \tag{2.11}$$

Thus τ, the radial phase shift, is independent of the energy W as long as $|W| < 1/r_0$. A phase shift of τ in the radial wave from H implies that the pure f wave of hydrogen is replaced by $f(k, r) \cos \tau + g(k, r) \sin \tau$. Thus the bound state wavefunctions are given by

$$\psi = f(l, \nu, r) \cos \tau + g(l, \nu, r) \sin \tau. \tag{2.12}$$

In this form the wavefunction satisfies the boundary condition of the correct radial phase shift τ at $r = r_0$ instead of the $\psi \to 0$ as $r \to 0$ condition of hydrogen. This is shown in figure 2. The requirement that $\psi \to 0$ as $r \to \infty$ is equivalent to requiring that the coefficient of $u(\nu, r)$ be zero. This leads to

$$\cos \tau \sin(\pi\nu) - \sin \tau \cos(\pi\nu) = 0 \tag{2.13}$$

or $\sin(\pi\nu - \tau) = 0$. Thus $\pi\nu - \tau$ must be an integral multiple of π, and $\nu = n + \tau/\pi$ where n is an integer. The effective quantum number ν of an Na state of angular momentum l differs from an integer by an amount τ/π which is usually termed the quantum defect and labelled μ. Since τ is independent of W, the quantum defect of a series of l states is a constant. As the radial wavefunctions for non-hydrogenic atoms obey the same $r \to \infty$ boundary condition they are similar to hydrogenic wavefunctions at large r, but they do have different energies.

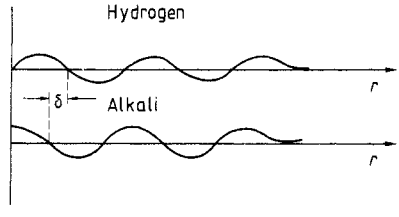

Figure 2. Wavefunctions of hydrogen and alkali atoms. The lower potential of the alkali introduces the radial displacement δ, due to the phase shift τ, as shown, leading to the depression of the energies of alkali low-l states relative to H.

The interesting aspects of Rydberg atoms stem mostly from their size, and with this in mind we turn to a closer inspection of the radial wavefunctions. The outer classical turning point is $2n^2$ while the inner classical turning point is approximately $l(l+1)$, and the radial function $rR_{nl}(r)$ oscillates with an amplitude which increases as $r^{1/4}$. The expectation values of positive powers of r depend primarily on the large-r part of the wavefunction and are thus independent of l (for low l). For low l

$$\langle r^k \rangle \propto n^{2k}. \tag{2.14}$$

Expectation values of inverse powers of r depend on the small-r part of the wavefunction and are hence dependent on l, which determines the inner classical turning point, $l(l+1)$. In spite of a very sharp l dependence, the expectation values of all inverse powers of r scale as n^{-3}, a consequence of the $n^{-3/2}$ normalisation of the radial wavefunction.

Although a knowledge of the scaling laws for radial properties is invaluable, it is frequently necessary to calculate specific radial matrix elements. This is in fact a rather straightforward proposition. It was first done by Bates and Damgaard (1949) who tabulated the radial matrix elements of r for electric dipole transitions. A somewhat different approach was adopted by Zimmerman *et al* (1979) who used a Numerov technique to evaluate bound radial matrix elements. The Numerov integration procedure is started for a decaying exponential in the classically forbidden large-r region. The integration is carried out for both wavefunctions of the matrix element to the inner turning point at which point it is stopped. As the Numerov solutions are generated the radial matrix element between two wavefunctions is generated as well as normalisation integrals for the two wavefunctions. In the first applications of this method a logarithmic transformation was applied to r so that more points would be used where the oscillations were more rapid. This was later refined by Bhatti *et al* (1981) to a square root transformation which allows the same number of points between successive nodes of the wavefunction.

The above method has been most useful for the calculation of bound wavefunctions. However, some problems, such as photoionisation and autoionisation, entail the use of continuum waves as well. This presents a slightly different problem. A bound wavefunction is completely specified by l and W, for the phase τ is implicitly defined by W. For continuum waves this is no longer true. Thus some reliable method of introducing τ must be found. A reasonable approach (Spencer 1981, Spencer *et al* 1982) is to begin the Numerov procedure at $r=0$ with the hydrogenic f wave and integrate out to some point where the kinetic energy is much larger than the Coulomb energy. At this point the radial phase of the wavefunction is shifted by τ. Now the wavefunction can be integrated back to $r=0$ to calculate the desired matrix elements.

The Numerov approach has been very successful in calculating matrix elements of all positive powers of r. However, since the radial wavefunctions are truncated at some small r, it is clear that matrix elements of r^{-k} cannot be calculated reliably for anything but H. However, in this case it works quite well, even for both bound-bound and bound-continuum matrix elements (Gallagher *et al* 1982).

2.1. Energy levels

In figure 3 we show the energy levels of H and Na. All the H angular momentum states of the same n are degenerate, whereas for Na only the higher l states are degenerate on the scale of figure 3. The lower l states are depressed in energy below

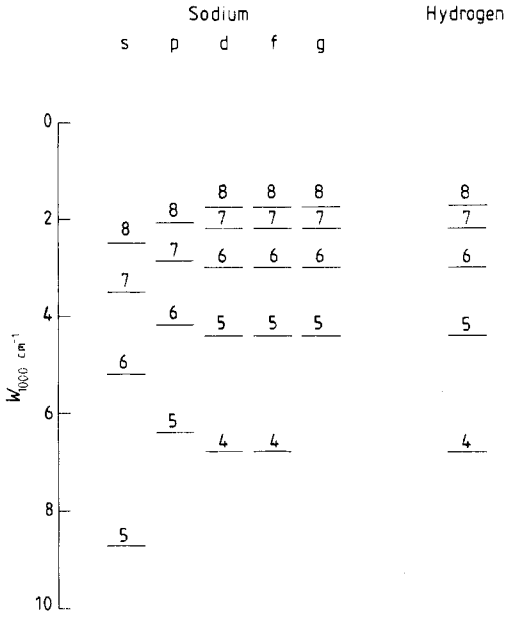

Figure 3. Energy level diagram for H and Na.

the hydrogenic values. Specifically the quantum defects of the s, p, and d states are 1.35, 0.85, and 0.01 respectively. The large quantum defects of the low-l states are due to penetration of the Na^+ core by the valence electron. In these states the electron probes the non-Coulomb part of the potential of figure 2. Only the lowest l states actually penetrate the core; the higher l states are excluded from the core by the $l(l+1)/r^2$ centrifugal potential. Even though the high-l Rydberg electrons do not penetrate the core, they do polarise it, and this also leads to non-zero quantum defects. The largest term is the dipole polarisation energy which is given by (Mayer and Mayer 1933)

$$W_d = -\tfrac{1}{2}\alpha_d\langle r^{-4}\rangle. \tag{2.15}$$

Here α_d is the dipole polarisability of the ion core and $\langle r^{-4}\rangle$ is the expectation value of r^{-4} for the Rydberg electron, which is the square of the electric field from the valence electron at the ion core. For H, or non-penetrating states generally, $\langle r^{-4}\rangle$ is given approximately by $3/(2n^3l^5)$ (Bethe and Salpeter 1957). The quantum defect of a non-penetrating state is related to the polarisation energy W_d by

$$\mu_l n^{-3} = -W_d. \tag{2.16}$$

Thus the quantum defect can be expressed in terms of the core polarisability and l as

$$\mu_l = 3\alpha_d/4l^5. \tag{2.17}$$

Thus if enough l intervals are measured to determine the core polarisability, all the higher l quantum defects may be determined using (2.17). Equation (2.15) is an excellent approximation for alkali atoms with one electron outside a closed-shell core, but for open-shell cores a more sophisticated approach must be used (van Vleck and Whitelaw 1933), which reduces to (2.15) for alkali-like atoms.

Table 2. Properties of Rydberg atoms.

Property	n dependence	Na(10d)
Binding energy	n^{-2}	0.14 eV
Energy between adjacent n states	n^{-3}	0.023 eV
Orbital radius	n^2	147 a_0
Geometric cross section	n^4	68 000 a_0^2
Dipole moment $\langle nd\|er\|nf\rangle$	n^2	143 ea_0
Polarisability	n^7	0.21 MHz cm^2 V^{-2}
Radiative lifetime	n^3	1.0 μs
Fine-structure interval	n^{-3}	−92 MHz

If we examine the fine structure we find that in H the interval between the $j=l+\frac{1}{2}$ and $l-\frac{1}{2}$ states is given by (Bethe and Salpeter 1957)

$$W_+ - W_- = \alpha^2/2l(l+1)n^3. \tag{2.18}$$

Here α is the fine structure constant, $\frac{1}{137}$. Note that the $j=l+\frac{1}{2}$ state is above the $j=l-\frac{1}{2}$ state, and that states of the same j are degenerate. In the Na or Cs atoms the fine structure intervals are similar to H for high angular momentum states, but vastly different for low-l states. In the Cs p states, for example, the fine structure intervals are three orders of magnitude larger than in H (Moore 1947). A most interesting observation is that the highest l state which penetrates the core typically has inverted fine structure (the $j=l+\frac{1}{2}$ state lies below the $j=l-\frac{1}{2}$ state). This is true in the Na and K d states and in the Rb and Cs f states (Fabre *et al* 1975, Gallagher and Cooke 1978, Farley and Gupta 1977, Fredriksson *et al* 1980). The Na f states on the other hand have fine structure intervals within 5% of the hydrogenic values (Gallagher *et al* 1977a). To date the fine structure intervals of the Rb and Cs g states can only be said to have magnitudes less than or equal to those of H.

The hydrogenic fine structure interval is due to the spin-orbit interaction which depends on the orbital radius as r^{-3}. As previously noted this leads to an n^{-3} dependence. In an alkali atom the fine structure interval is derived from the interaction of the valence electron with the core. Specifically it is thought to be a polarisation of the core electrons, which depends on having non-zero angular momentum in the core electrons (Sternheimer *et al* 1976). This notion is supported by the hydrogenic fine structure intervals of the Li nd states (Cooke *et al* 1977). In any case the interaction is dominated by the short-range interaction between the electron and the core, depending upon an inverse power of r, and again exhibits an n^{-3} dependence.

In general, most of the properties of Rydberg atoms depend upon some combination of radial matrix elements and energies. Thus it is possible to develop simple n-scaling laws for these properties. In table 2 we list some of these properties, their n scaling, and values for the Na 10d state. Some of the properties, such as the geometric cross section, are obvious. The origin of the others should become clear in subsequent sections.

3. Atoms in strong electric fields

The easiest place to begin a discussion of atoms in strong fields is the hydrogen atom. If we ignore the spin-orbit interaction and the fact that there are small electric dipole

couplings between adjacent n manifolds, the Stark effect in hydrogen reduces to a very tractable problem. If an electric field E is applied in the z direction, the state nlm is coupled to the two states $n, l \pm 1, m$. Thus the Hamiltonian matrices for different m are separate. Furthermore in the matrix for any m the diagonal matrix elements are all $-1/2n^2$ and may be subtracted, leaving a symmetric, purely off-diagonal matrix, all the entries of which are proportional to E. Thus all the eigenstates in the field have electric field shifts which are linear in the electric field. In other words the Stark eigenstates obtained by diagonalising the Hamiltonian matrix have permanent dipole moments, unlike the familiar nlm states. Physically this corresponds to the fact that in the Stark states the average z position of the electron is not zero but varies from $z = -\frac{3}{2}n^2$ to $z = +\frac{3}{2}n^2$ in the possible states of principal quantum number n.

For the hydrogen atom in an external field the Schrödinger equation may be separated in parabolic coordinates yielding directly the wavefunctions and energies (Bethe and Salpeter 1957). Conventionally the quantum numbers n, n_1, n_2 and m are used to describe the Stark states. The parabolic numbers n_1 and n_2 can take the values $n - |m| - 1$ and are further constrained by the requirement that

$$n_1 + n_2 + |m| = n - 1. \tag{3.1}$$

The first-order energies of the Stark states are given by

$$W = -1/2n^2 + \tfrac{3}{2}En(n_1 - n_2). \tag{3.2}$$

While there is no explicit m dependence in (3.2), it enters in two ways. First, (3.1) constrains even and odd m states to be interleaved; they cannot be degenerate. Second, as $|m|$ is increased the maximum possible values of n_1 and n_2 decline, with the result that the maximum Stark shift declines with $|m|$. The extreme case is of course the circular state $|m| = n - 1$ for which $n_1 = n_2 = 0$ and the first-order Stark shift vanishes.

The n, n_1, n_2, m Stark states can also be obtained by diagonalising the Hamiltonian of the n, l, m states in an external field. Not surprisingly, this transformation has a simple form (Park 1960):

$$\langle \psi_{nn_1n_2m} | \psi_{nlm} \rangle = (-1)^m (2l+1)^{1/2} \begin{pmatrix} \frac{1}{2}(n-1) & \frac{1}{2}(n-1) & l \\ \frac{1}{2}(m+n_1-n_2) & \frac{1}{2}(m-n_1+n_2) & -m \end{pmatrix} \tag{3.3}$$

where the term in the large parentheses represents a Wigner $3J$ symbol.

In the hydrogen atom the consideration of only the first-order Stark effect is usually adequate, even up to the fields at which the atom ionises, and this may be used to develop a quantitative insight into the process of field ionisation. In figure 4 we show the potential along the z axis for an atom which is in an electric field E of 5×10^{-7} au (2700 V cm^{-1}). Classically, field ionisation is allowed whenever the energy of a state exceeds the energy of the saddle point of the potential. In a Coulomb $1/r$ potential this occurs when the binding energy measured relative to the zero-field limit is

$$|W_c| = 2E^{1/2}. \tag{3.4}$$

If we ignore the Stark shifts of the levels this leads to the often-stated law

$$E_c = 1/16n^4 \tag{3.5}$$

as the classical limit for ionisation. There are two factors which cause H to deviate from this rule, the Stark shifts and the spatial distribution of the electron wavefunction. First let us consider the latter point, focusing on the extreme upwardly blue-shifted Stark state and the extreme downwardly red-shifted Stark state of the same n. The

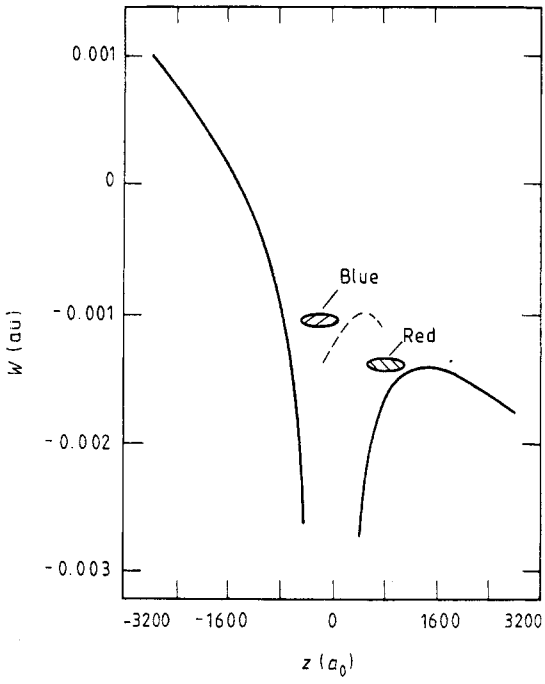

Figure 4. Potential along the z axis when a field of 2700 V cm^{-1} is applied to the atom. The red and blue wavefunctions are localised as shown. The blue wavefunction is localised by the barrier, indicated by the broken curve, which is analogous to a centrifugal barrier.

electrons are localised on the high- and low-potential sides of the atom as shown by figure 4. The blue state is confined to its location by something analogous to a centrifugal barrier which is shown by the broken curve. The red-shifted state is similarly confined to the region near the saddle point. An important difference is that in the red Stark state the electron is localised in the region of the saddle point over which it must escape from the atom. The energy of the red state in the field is given by

$$W = -\frac{1}{2n^2} - \tfrac{3}{2}n(n-1)E. \tag{3.6}$$

Setting $n-1 \approx n$ and equating this energy to our previous requirement for ionisation, (3.4) leads to the simple result

$$E_H = 1/9n^4. \tag{3.7}$$

This ignores tunnelling, but since tunnelling rates change exponentially with field, (3.7) gives a prediction in excellent agreement with experimental results.

At the same field the blue Stark states are quite stable in spite of having an energy far above the saddle-point energy. This is entirely due to the electron being constrained to be on the high-potential side of the atom, away from the saddle point. While we have no simple picture to explain ionisation of the blue Stark states, we note that the fields required for the extreme blue Stark states of $n \sim 15$, are typically a factor of two higher than for the extreme red Stark states of the same n (Bailey *et al* 1965). In figure 5 we show the Stark effect and ionising fields of hydrogen $n \sim 10$, $m = 0$ states, as well as the extreme $n = 9$ and $n = 11$ states. Note that the red states ionise at the classical ionisation limit while the blue states do not.

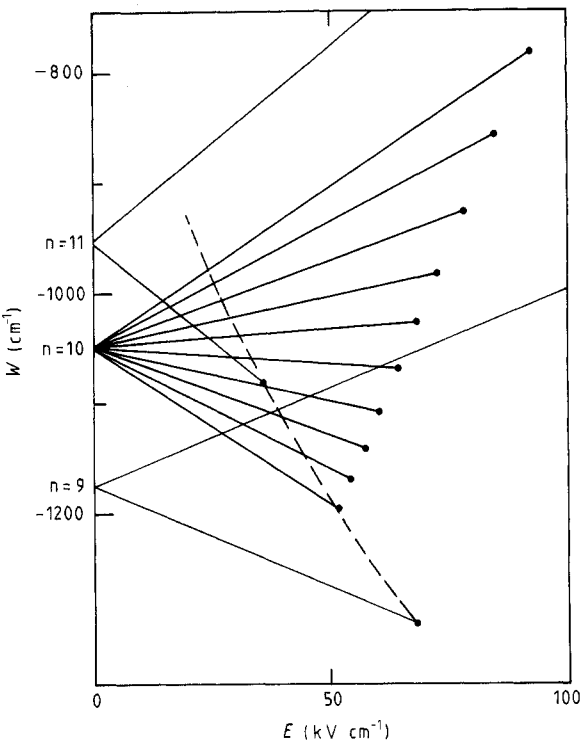

Figure 5. Energy levels of H, $m = 0$, in an electric field. All $n = 10$ levels are shown as are the extreme $n = 9$ and $n = 11$ levels. The points (●) represent an ionisation rate of $\sim 10^9\ s^{-1}$. The broken curve is the classical limit for ionisation. Note that the red states ionise at the classical limit and that the levels of adjacent n cross.

Atoms other than hydrogen exhibit in some cases identical and in others strikingly different properties from those of hydrogen. We can decide whether the properties will be hydrogenic or not by first recalling that an electric field in the z direction couples state (n, l, m) to states $(n', l \pm 1, m)$, i.e. states of different m are not coupled. Now if we examine the energy level diagrams of Na, for example, shown in figure 4, we can see that the $l > 2$ states are degenerate, with the hydrogenic energy $-1/2n^2$, while the s and p states lie between the hydrogenic levels. Thus if we consider $|m| = 2$ levels, only the hydrogenic $l \geqslant 2$ levels are involved. As the $l \geqslant 2$ states are largely hydrogenic, the preceding treatment of hydrogen in a field applies. Certainly the energy levels can be calculated to high accuracy using the hydrogenic expression and, as we shall see, many of the Na $|m| = 2$ properties are hydrogenic.

The $|m| = 0$ states on the other hand include the s and p levels which are clearly not degenerate with the higher l states. This has two complicating effects which become painfully apparent when we begin to write down the Hamiltonian matrix. The fact that the Na s and p states have energies halfway between the hydrogen-like n and $n-1$ manifolds of higher l states means that the wavefunctions are also halfway between n and $n-1$ wavefunctions. Thus the dipole matrix elements connecting the ns to np and $(n-1)$p states are comparable, as are those connecting np to nd and $(n-1)$d states. In sum there are strong dipole couplings between adjacent manifolds, unlike hydrogen, and we cannot treat the Stark manifolds of different n as being independent. Even if we do so at low field, the fact that the l states of the same n are

no longer degenerate means that a common energy of $-1/2n^2$ cannot be subtracted from all states to leave a purely off-diagonal matrix proportional to E. Thus the Stark effect is no longer linear.

The energy levels and wavefunctions for the $m = 0$ states may be determined by diagonalising the $|m| = 0$ Hamiltonian matrix for several n states, i.e. following the procedure mentioned at the beginning of this section (Zimmerman *et al* 1979). How many states are required depends on the field strength and the desired accuracy. In figure 6 we show the Na energy $m = 0$ levels for $n \sim 15$ (Littman *et al* 1976). Although the qualitative resemblance to hydrogen is clear there are two obvious differences. First, the s and p states have minimal Stark shift until they approach the Stark manifold, at which point they become part of the manifold. The second is the fact that the blue $n = 15$ levels do not cross the red $n = 16$ levels, but exhibit obvious avoided crossings, a phenomenon which does not occur in hydrogen.

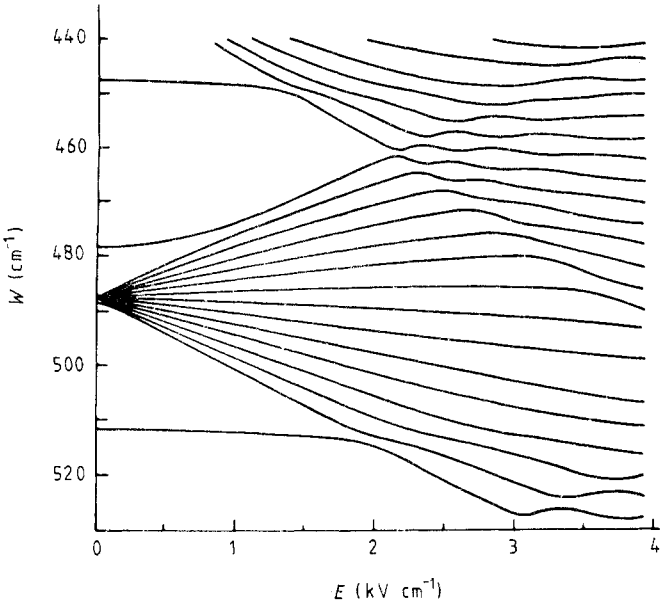

Figure 6. Na $m = 0$ levels near $n = 15$. Note in particular the avoided crossings of the levels (Littman *et al* 1976).

The magnitudes of the avoided crossings are proportional to the energy matrix element coupling the zeroth order $n = 16$ red and $n = 15$ blue states. For any matrix element to be non-zero requires some spatial overlap of the two wavefunctions. In hydrogen the blue and red wavefunctions do not overlap at all, hence the couplings leading to avoided crossings vanish, at least non-relativistically. For Na the Stark states do not have the complete localisation on one side of the atom or the other as do the hydrogen Stark states with the result that the red states have some blue character and vice versa. Consequently the red $n = 16$ Stark states are coupled to the blue $n = 15$ Stark states resulting in the avoided crossings of figure 6.

The fact that the wavefunctions of $m = 0$ states of Na can never be entirely localised away from the saddle point simplifies the static field ionisation. There is always some wavefunction at the saddle point and thus ionisation occurs in a completely classical

fashion as given by (3.4). Stated another way the field required for ionisation is

$$E_c = (W/2)^2 \tag{3.8}$$

where W is the binding energy relative to the zero-field ionisation limit.

The classical ionisation at the saddle point can be understood in terms of wavefunctions in the following manner. As shown by figure 6, there are very obvious avoided crossings between the Na Stark states of adjacent n manifolds, and this is indicative of substantial mixing of the wavefunctions. Thus each Na level is a mixture of higher-n red Stark states and lower-n blue Stark states. The ionisation occurs through the ionisation of the higher-n part, and it is the amount of mixing with this state that partially determines the ionisation rate. Thus the process is more like autoionisation than tunnelling (Littman *et al* 1978). Only when the field required for hydrogenic ionisation is reached does an atom decay directly by field ionisation.

3.1. Dynamic effects in time-varying fields

One of the more important examples of Rydberg atoms in time-varying fields is the pulsed field ionisation method used to selectively detect specific Rydberg states. It is also interesting in itself as an excellent example of how the static-field dependence can be used to understand the dynamics of time-dependent processes. Many, if not most, experiments involving Rydberg atoms are designed to investigate processes, such as collisions, which occur in low or zero static fields. However, pulsed field ionisation is frequently employed to detect the Rydberg atoms in a state-selective manner. There are really two aspects to pulsed electric field ionisation. One is the passage from zero field to the high ionising field and the other is the ionisation itself, which we have already discussed.

How atoms pass from zero field to high field is determined by the energy levels in a static electric field and the slew rate of the field. The only question is whether the passage is diabatic or adiabatic. If the slew rate of the field is such that the time t_0 required to traverse a typical Stark level crossing is long compared to the inverse of the size ω_0 of the crossing, $t_0 \gg 1/\omega_0$, the passage from low to high field is likely to be adiabatic. If on the other hand the time to traverse a crossing is short, $t_0 \ll 1/\omega_0$, then the passage is likely to be diabatic. Cases in which the passage from low to high field is neither purely adiabatic or diabatic also occur and are difficult to unravel.

Let us examine H first. If we imagine that at $t = 0$ we have a zero field n, l, m state, applying any field should project this state onto the set of n, n_1, n_2, m states implied by (3.3), i.e. the transition is by definition diabatic. If on the other hand we start with a very low field, $\sim 1\ \mathrm{V\ cm^{-1}}$, at $t = 0$ then the atom is in a well defined n, n_1, n_2, m state, and we can now ask what will happen to this atom as we raise the field to the value at which the atom is ionised. What happens depends, of course, on the risetime of the field. We can restrict our attention to the case of practical interest in which the field pulse rises in a time short compared to the radiative lifetime of the Rydberg state. This usually means risetimes $\leq 1\ \mu\mathrm{s}$.

The passage from low to high field can be understood easily with the aid of the Stark energy diagram of figure 5. As the field is increased the energy of the atom changes, and for fields above $40\ \mathrm{kV\ cm^{-1}}$ in figure 5 the atom encounters level crossings with states of higher and lower n. As these crossings indicate no interaction, the atom passes through them unaffected until it reaches the point at which it ionises. Here we have ignored the fact that there are small couplings produced by the spin-orbit effects.

In H the spin-orbit splittings are comparable to the radiative decay rates, so the level crossings are traversed in times much shorter than the radiative decay rates with the result that the traversal is diabatic, and the spin-orbit effect may be safely ignored. For the hydrogen atom we reach the remarkable conclusion that ionisation occurs at the same field value for static, pulsed or oscillating fields up to a frequency about an order of magnitude smaller than the $n \rightarrow n+1$ interval, at which point multiphoton transitions begin to occur.

If we examine atoms other than H we find a different situation, but the same method of analysis applies. The states of non-zero quantum defect couple the Stark states of different n, leading to large avoided crossings between Stark states of adjacent n, radically altering the atom's response. As an example we consider the 17d state of Na, which provides excellent insights into the process (Gallagher *et al* 1977c).

In the first 10 V cm^{-1} of a typical field pulse, which turns on slowly, the atoms pass adiabatically from the zero field $n\mathrm{d}_{3/2}$ or $n\mathrm{d}_{5/2}$ state to a state in which the spin and orbital angular momenta are decoupled. This state is characterised by angular momentum quantum numbers l, m, s, m_s. In the adiabatic passage, each zero-field or low-field $lsjm_j$ state passes to one $lmsm_s$ state, while preserving the value of $m_j = m_s + m$. If the field rises to $\sim$10 V cm^{-1} rapidly compared to the fine structure splitting, the $lsjm_j$ states are simply projected onto the $lmsm_s$ states as described by a Wigner 3J symbol. Note that in this case a single $lsjm_j$ state is projected onto several intermediate-field $lmsm_s$ states. At this point the spin is decoupled from the orbital angular momentum, and the spin may from this point on be neglected. Since the d-f interval is large, $\sim$1 cm^{-1}, compared to the rate of time variation of the pulse, as the field is raised above 10 V cm^{-1} the atom adiabatically passes from the 17d state to a Stark state, and decreases in energy as shown by the bold line of figure 7, always keeping the same value of m. For

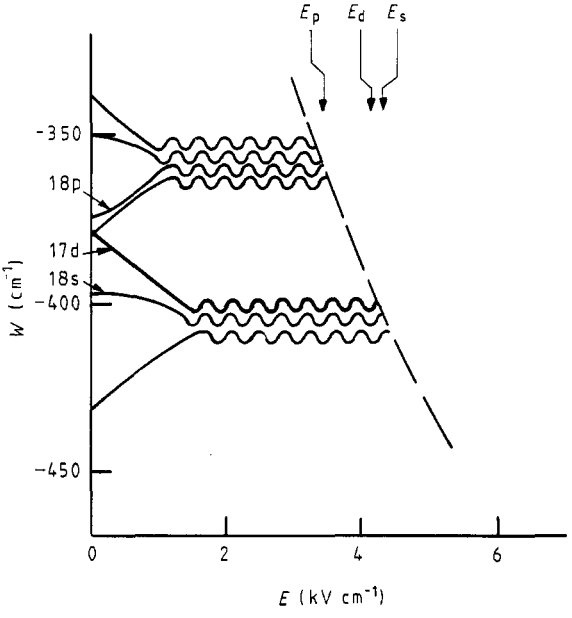

Figure 7. Energy levels of Na in a field showing by the bold line the adiabatic path to ionisation of an atom initially excited to the 17d state. The atom ionises at the classical ionisation limit, indicated by the broken line, at field E_d. Following analogous adiabatic paths for the 18s and 18p states leads to ionisation at fields E_s and E_p respectively.

concreteness we shall assume that we have an $m=0$ state. When the field reaches ~ 1 kV cm^{-1} the atom encounters an avoided crossing with a blue shifted $n=16$ state. Since the $m=0$ avoided crossings at $n\sim 17$ are ~ 1 cm^{-1} and times of at least 10 ns are required to traverse the crossings, the crossing is traversed adiabatically as are the subsequently encountered crossings of figure 7. The net result is that the atom passes adiabatically to the classical field for ionisation at which point it ionises. An important point to note is that the path of the 17d state is trapped between the $n=16$ and $n=17$ manifolds and thus fixed in energy at -403 cm^{-1} for $E>1$ kV cm^{-1}. Similar reasoning can be applied to the 18s state, which will eventually ionise at field E_s, and to the 18p state which ionises at E_p. If we examine the $n=17$, $l>2$ states of Na, they ionise at fields between E_p and E_d. From figure 7 it is apparent that it is the binding energy at the ionising field, not the zero-field binding energy, which is important in determining the ionising field. Thus while the 17d and 18p states have similar zero-field energies they ionise at very different fields.

In figure 7 we have shown only $m=0$ states, but the same arguments can be applied to the $|m|=1$ states. Consider two states of the same binding energy but of $|m|=0$ and 1. The $|m|=1$ state is slightly harder to ionise due to a centrifugal barrier. The saddle point in the potential occurs on the z axis, $x=y=0$, from which the $|m|=1$ electron is excluded by a centrifugal barrier. Thus the $|m|=0$ state can ionise at a slightly lower field. The same arguments can be extended to higher $|m|$ and have been worked out in a quantitative fashion (Cooke and Gallagher 1978).

The above picture describes Na states up to $n=17$ perfectly for ~ 1 μs risetime pulses. The picture begins to break down at $n=18$ for $|m|=2$ states. The $n=18$–19, $|m|=2$ avoided crossings are estimated to be ~ 0.01 cm^{-1}, and they are traversed in times of 1 ns, so it is clear that the adiabatic criterion is only marginally met. As n is increased, the $m=2$ states revert to hydrogenic behaviour. Above $n=18$ the $|m|=2$ states traverse some crossings in a partially diabatic fashion leading to multiple ionisation threshold fields (Gallagher *et al* 1977c). By $n\sim 35$ the passage through the high-field regime has become purely diabatic and one threshold, at the hydrogenic value of $1/9n^4$, is observed (Jeys *et al* 1980).

In Na the fine structure splitting is small enough that the coupling between $|m|$ states produced by it is negligible, allowing us to ignore the electron's spin. This is not true for the heavier alkali atoms. In Rb and Cs multiple thresholds are observed, due to the spin–orbit mixing of m and $m\pm 1$ states (Gallagher *et al* 1981). An interesting case is K, which shows a mixing of the $|m|=0$ and 1 states but not of the $|m|=2$ states, a reflection of the large p fine structure interval (Gallagher and Cooke 1979a).

3.2. Microwave fields

Historically the microwave ionisation of Rydberg atoms was studied with the goal of linking photoionisation and field ionisation (Bayfield and Koch 1974). In hydrogen, as we have pointed out, there is essentially no room for dynamic effects until the frequency of the microwave field is within an order of magnitude of the Δn spacing. This is apparently the case as shown by figure 8, a plot of ionisation field against n at 9.9 GHz (van Leeuwen *et al* 1985). The scaled ionising field n^4E remains at $1/9n^4$ until $n=40$, corresponding to $n^3\omega=0.1$ in figure 8, where it starts to decrease. The Δn separation is 103 GHz at $n=40$ decreasing as $1/n^3$ to 18 GHz at $n=70$, corresponding to $n^3\omega=0.5$ in figure 8. For a 9 GHz microwave frequency 30 GHz corresponds approximately to three photons, and it is probable that ionisation at this point occurs

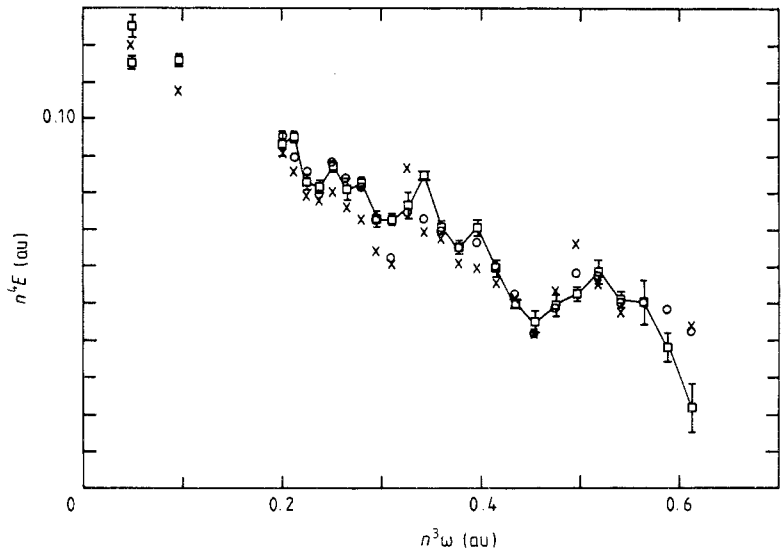

Figure 8. Scaled microwave ionisation field, n^4E, for hydrogen, plotted against the scaled microwave frequency $n^3\omega$: experimental (□); one-dimensional theory (×); two-dimensional theory (○). $n^3\omega = 0.05$ corresponds to $n = 32$ and $n^3\omega = 0.6$ corresponds to $n = 73$. Note the decline from $n^4E = \frac{1}{9}$ at $n = 30$ to progressively lower values as n approaches 60 (van Leeuwen *et al* 1985).

via multiphoton transitions to higher n states. Such transitions have been studied explicitly and are observed at microwave fields comparable to the ionising fields for these values of n (Bayfield *et al* 1977).

Atoms other than hydrogen exhibit a radically different form of ionisation. For example Na $m = 0$ and 1 atoms exhibit ionisation threshold fields given by (Pillet *et al* 1983b):

$$E = 1/3n^5 \tag{3.9}$$

and He shows similar behaviour in rapidly varying fields (Mariani *et al* 1983). This can be readily understood in terms of the static energy levels, as shown by figure 9. Consider an initially excited $n = 20$d atom in an $m = 0$ state which is exposed to a microwave pulse. Early in the pulse the 20d state is mixed with the other $n = 20$, $l > 2$, $m = 0$ states, and as a result some (statistically one in eighteen) of the atoms are in the highest-energy Stark state. When the microwave field amplitude reaches 600 V cm^{-1} these atoms are brought to the avoided crossing with the lowest-energy $n = 21$ state, and they can make a Landau-Zener transition to the $n = 21$ state. As shown by figure 9 the fields at which higher Stark manifolds intersect are lower, so that having made the transition to $n = 21$ it is possible to continue making $\Delta n = +1$ transitions and eventually ionise at the classical ionisation limit. On the other hand the intersection of the $n = 20$ and $n = 19$ Stark manifolds occurs at a higher field so it is clear that the only path available to the $n = 20$ atom is toward ionisation. The threshold field for ionisation corresponds to the intersection of the $n = 20$ and $n = 21$ Stark manifolds which occurs at $E = 1/3n^5$ for $m = 0$ states. To make the $n \rightarrow n+1$ Landau-Zener transition at an avoided crossing requires that it be traversed in a fashion that lies between the adiabatic and diabatic limits, i.e. the time must be comparable to the inverse of the size of the avoided crossing. Since there are as many as 10 000 microwave

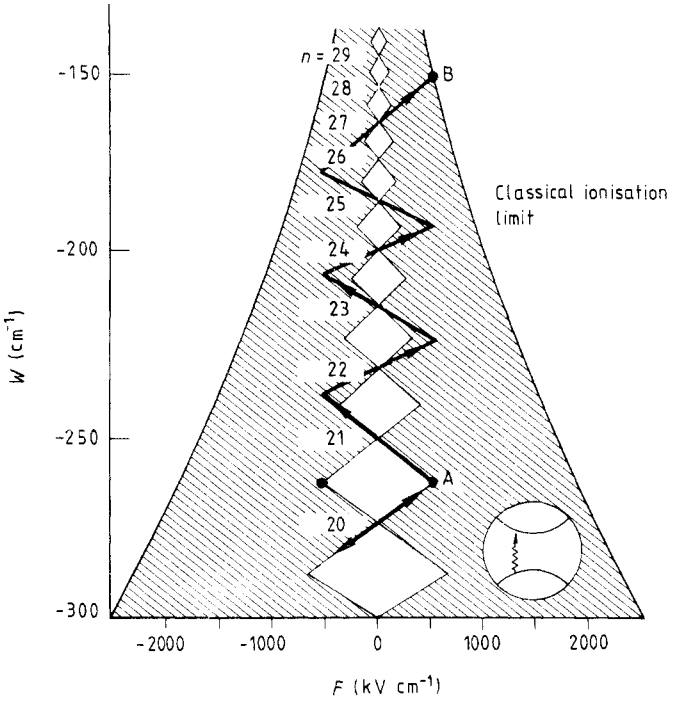

Figure 9. Na energy level diagram showing the microwave ionisation of the Na 20d state. An oscillating microwave field mixes the $n = 20$ states so that some are in the extreme blue state. If the microwave field amplitude reaches point A, at $E = 1/3n^5$, an atom in the blue $n = 20$ state can undergo a Landau-Zener transition to the $n = 21$ red state at the avoided crossing shown in the inset. Similar $\Delta n = 1$ transitions subsequently occur culminating in ionisation at point B (Pillet *et al* 1984).

cycles in a typical experiment the probability of making a transition on ány given cycle need not be high, and therefore the match between the avoided crossing size and the microwave frequency is a very loose requirement (Pillet *et al* 1984).

4. Interaction with radiation

A natural starting point for a discussion of the interaction of Rydberg atoms with radiation is the radiative lifetime, which is a reflection of the coupling to the vacuum fluctuations. The radiative decay rate, $1/T$, of state n is given by the sum of Einstein A coefficients (Bethe and Salpeter 1957):

$$\frac{1}{T} = \sum_{n'} A_{nn'} = \sum_{n'} \tfrac{4}{3}\alpha^3 \omega_{nn'}^3 \mu_{nn'}^2 \frac{g_>}{2g_n + 1} \tag{4.1}$$

where $\mu_{nn'}$ is the dipole matrix element connecting states n and n', $\omega_{nn'} = W_n - W_{n'}$ is the energy difference between the two states, g_n and $g_{n'}$ are the degeneracies of states n and n', and $g_>$ is the larger of g_n and $g_{n'}$. In (4.1) the sum extends over all states n' for which $W_n > W_{n'}$.

In figure 10 we show the individual values of $A_{nn'}$ for the decay of the Na 18s state to lower-lying np states as the hatched bar graphs. The behaviour of figure 10 is typical

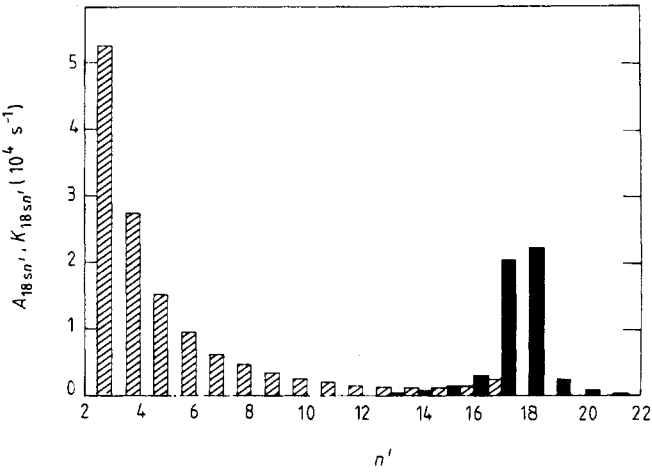

Figure 10. Spontaneous emission rate $A_{18sn'}$ (hatched bars) of the Na 18s state to n'p states and the 300 K black-body transition rate $K_{sn'}$ (full bars) as a function of n' (Gallagher 1982).

of most low angular momentum Rydberg states. They have a whole range of possible decay transitions from millimeter wave to ultraviolet. Generally the shortest wavelength transition dominates, due to the $\omega^3_{nn'}$ factor. For Rydberg states, the change in frequency of the shortest wavelength transition with n is very small and may be neglected. The n dependence thus originates entirely in the dipole matrix elements. The dipole matrix element between the ground state and a Rydberg state only depends upon the small-r part of the Rydberg state wavefunction which overlaps with the ground-state wavefunction near the ion core. The only change in this part of the Rydberg state wavefunction with n is the normalisation, scaling as $n^{-3/2}$. Thus the radial matrix element scales as $n^{-3/2}$ and its square as n^{-3} leading to radiative decay rates scaling as n^{-3} or lifetimes scaling as n^3.

If we consider the opposite extreme of the high l states, they have only one possible decay, to the next-lower n state. In this case $\omega_{n,n-1} = 1/n^3$, and the dipole matrix elements connecting the n and $n-1$ states reflect the size of the Rydberg states and scale as n^2. Thus the radiative decay rates scale as n^{-5}, and the lifetimes as n^5. As pointed out by Bethe and Salpeter (1957) the average lifetime of all lm states of the same n is observed to scale as $n^{4.5}$. This has been recently derived analytically by Chang (1985).

The n^{+3} dependence of the radiative decay times of low-l states, which are readily accessible by laser excitation, has been confirmed for several atoms over a range of roughly two orders of magnitude in lifetime (Gallagher *et al* 1975). The n^5 variation of the lifetime for the highest l states has not been observed explicitly, but collision experiments have been carried out in which mixtures of nearly all l, m states of the same n are observed to decay with a rate scaling as $n^{4.5}$ (Gallagher *et al* 1977b).

Until a few years ago all experiments with Rydberg atoms were done at room temperature, 300 K, or above and, based on the A values of figure 10, it was assumed that there would be negligible radiative decay to nearby lower Rydberg states, and of course none to higher Rydberg states. In fact at 300 K the black-body radiation alters the total radiative decay rate as shown for the Na 18s state by the full bar graph of figure 10 (Gallagher 1982). At a finite temperature there are $\tilde{n}$ photons per mode in

the thermal radiation field so the A values of (4.1) must be multiplied by $\bar{n}$ to obtain the stimulated emission rates (Loudon 1973). In addition, the possibility of absorption must be added to the decay rate, thus the sum of (4.1) must be extended to include higher-lying states as well. The effect of black-body radiation is largest for low-frequency transitions, i.e. $\hbar\omega < kT$, for which $\bar{n} = kT/\hbar\omega$. For the low-l states, such as the Na 18s state, which decay predominantly by short-wavelength transitions, roughly 20% of the atoms are transferred to nearby states by black-body radiation, and the lifetimes are thus shortened by 20% (Beiting *et al* 1979, Cooke and Gallagher 1980). For the anomalously long-lived Na np states the observed lifetimes are found to be a factor of three shorter than expected on the basis of calculations ignoring black-body radiation (Gallagher and Cooke 1979b). For the highest l states, which can only decay by the $\Delta n = -1$ transition, the lifetimes are shortened by an order of magnitude, a factor equal to the photon occupation number $\bar{n} \sim kT/\hbar\omega$.

Population put into a single state by a laser is fairly rapidly distributed over nearby states by thermal radiation, making some kinds of experiments impossible at 300 K. In general, black-body radiation is a nuisance, the only exception being its use in anticrossing spectroscopy (Stoneman and Gallagher 1985). However, the detection of the absorption of thermal radiation, and subsequent measurements with FIR lasers did demonstrate that Rydberg atoms were indeed very sensitive detectors of low-frequency radiation (Gallagher and Cooke 1979c, Ducas *et al* 1979, Figger *et al* 1980). That this might be the case was first suggested by a series of microwave resonance measurements (MacAdam and Wing 1975, Gallagher *et al* 1976, Fabre *et al* 1977). It became clear in these measurements that very low powers, $\sim 10^{-10}$ W cm^{-2}, were required to drive single photon transitions.

Beyond the observable population transfer, the 300 K radiation has another effect. It produces a field of ~ 10 V cm^{-1} centred at ~ 3 kT, 1000 cm^{-1} at 300 K, and this field leads to a second-order AC Stark shift of the Rydberg levels. While it is straightforward to write out the shift as an infinite sum of contributing terms, in the limit of high principal quantum number, the frequency of the black-body radiation is high compared to the frequencies of the strong transitions of the Rydberg atom, and the expression reduces to the classical expression for the energy of a free electron in an oscillating field (Cooke and Gallagher 1980)

$$W = e^2E^2/2m\omega^2. \tag{4.2}$$

Physically this corresponds to a high-frequency oscillatory motion of the electron as it slowly goes around the ion core, and thus the energy is additive. At room temperature the shift is not large, 2 kHz, and since all Rydberg states experience the same shift it can only be observed from a low-lying state. In fact the thermal shift has been measured in an elegant two-photon absorption from the ground state of Rb to the Rydberg states (Holberg and Hall 1984). It is interesting to note that the black-body radiation AC Stark shifts alter the 9 GHz Cs hyperfine frequency used as the definition of the second to an almost perceptible degree (Itano *et al* 1982).

The interaction of black-body radiation with Rydberg atoms presents an interesting opportunity for controlling the interaction of an atom with radiation. Obviously changing the temperature directly changes the black-body transition rates, and this has been shown explicitly. On the other hand, the black-body radiation may be constrained to a small number of modes by the use of a high-Q cavity. Thus if the cavity is tuned to resonance with an atomic transition a substantial increase in the black-body transition rate is observed (Goy *et al* 1983). Similarly if the cavity is tuned

away from a resonance the black-body transition rate decreases. A special case of this occurs when the atomic frequency is tuned below the cutoff frequency of the waveguide structure in which the atom resides, suppressing the radiation at the atomic frequency. This leads to an abrupt decrease in the black-body transition rate as the atomic frequency is tuned below cutoff (Vaidyanathan *et al* 1982).

The same notions described above for the control of black-body radiation by cavities apply equally well to the vacuum fluctuations and, using a similar technique to the above, Hulet *et al* (1985) have observed the suppression of spontaneous emission of the circular $l = m = n - 1$ Rydberg states at a temperature of 4 K, where the effects of black-body radiation are negligible. For a circular state the $\Delta n = -1$ transition is the only possible radiative decay, so the effect of suppressing it is readily apparent in the total decay rate of the state.

It is quite easy to prepare enough atoms in a Rydberg state that there occurs what is usually termed superradiant emission to lower-lying states. Loosely, it is like a laser without mirrors. Not surprisingly this occurs when the sample of Rydberg atoms has appreciable gain, ~ 1, for a transition to a lower-lying level. However, black-body radiation, not spontaneous emission, triggers the superradiance, so the whole process may be thought of as amplified black-body radiation. This process occurs readily even with the very small number of Rydberg atoms that can be excited in an atomic beam. In fact whole sequences of cascades (Gounand *et al* 1979) have been used to populate normally inaccessible states and use them for experiments. In most cases the fact that superradiance has occurred is inferred from the rapid transfer of population between two Rydberg states and the dependence of the rate on the number of Rydberg atoms (Gross *et al* 1979). The radiation is usually not detected since it is only a small number of relatively low-frequency photons and therefore an insignificant amount of power.

Pursuing the previous notion of superradiance as a laser without mirrors, it is reasonable to suppose that putting the sample of Rydberg atoms in a high-Q cavity would allow one to make a maser with a substantially smaller number of atoms. The higher the Q of the cavity the smaller the number of atoms required to maintain an oscillation. Recently Meschede *et al* (1985) have demonstrated the ultimate example of this, a one-atom maser, using the Rb $63p$–$61d$ transition at 21 GHz in a superconducting cavity with a Q of 10^9. This opens the door to the study of a new very statistical maser, unlike any other practical masers or lasers.

5. Collisions

Since the Rydberg atoms are large, with orbital radii $\sim n^2 a_0$, it is hardly surprising that substantial attention has been focused upon their collisional properties. One might expect that the large size of the Rydberg atom would ensure correspondingly large collision cross sections. However, this is not always true. As we shall see, Rydberg atoms are quite transparent to many collision partners.

Rydberg atoms collisions can be divided into two categories, those in which the collision partner interacts with the atom as a whole and those in which it interacts separately with the Rydberg electron and the ion core. The distinction is based on the range of the interaction. In the case of short-range interactions, such as with ground-state atoms and molecules, the collision partner interacts separately with the Rydberg electron and the ion core. For long-range interactions, such as with charged particles, the collision partner interacts with the Rydberg atom as a whole. Collisions between

two Rydberg atoms also fit into the latter category, which is not completely surprising since a Rydberg atom is just two widely separated charged particles.

Let us consider for a moment a simple physical picture of a thermal collision between a Na Rydberg atom of $n \sim 10$ and a ground-state molecule. As shown by figure 11 the perturbing molecule M passes through an electron cloud, centred on the Na^+ ion core, where it can interact with both the Rydberg electron and the ion core. This is in essence a three-body problem with three interactions

$$e^-\text{-}M \qquad Na^+\text{-}M \qquad Na^+\text{-}e^-.$$

Ignoring for a moment the first two, the last of these simply defines the energy levels of the Na atom. The two interactions of the molecule M, with the electron and the Na^+, are both relatively short-range interactions. There is a very short-range part, almost corresponding to hard-sphere scattering, which is characterised by the low-energy scattering length for the Rydberg electron, and somewhat longer-range parts arising from the electrostatic interactions of the electron or Na^+ with the multipole and induced multipole moments of the molecule. For atoms, which generally have no permanent multipole moments in their ground states, only the induced moments exist. The important point is that for any noticeable interaction the molecule must be within a few ångströms of the electron or Na^+. Since the Rydberg electron cloud is substantially larger than the ion core, it determines the collision properties of the Rydberg atom in most cases. As a result many theoretical approaches are based on a binary encounter between the Rydberg electron and the colliding molecule, and most of the important collisional properties of Rydberg atoms can be related to low-energy electron–molecule and electron–atom scattering (Hickman *et al* 1982, Matsuzawa 1982, Flannery 1982, Omont 1977).

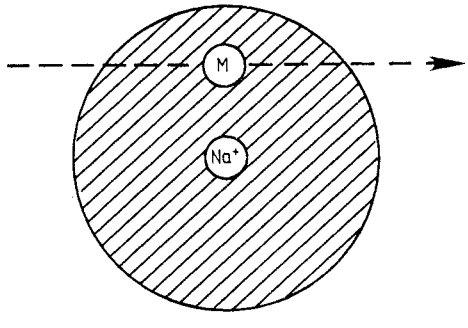

Figure 11. A molecule M colliding with a Rydberg atom which is composed of the Na^+ core and the diffuse electron cloud indicated by the hatched area.

Adopting the point of view that electron–atom or electron–molecule scattering determines Rydberg atom collision properties, we can now consider what are the energetically allowed final states of collisions. We begin with collisions between the Rydberg electron and a ground-state atom. The ground-state atom has no accessible internal degrees of freedom and can only increase or decrease its translational energy in a collision. A Rydberg electron colliding with an atom is roughly analogous to a ping pong ball bouncing from a bowling ball; there is little energy exchange due to the disparate masses of the two. The characteristic amount of energy transferred to the atom in thermal collision at temperature T is

$$\Delta W \sim 4kTv/V \tag{5.1}$$

where k is the Boltzmann constant, and v and V are the velocities of the Rydberg electron and colliding atom respectively. At an orbital radius anything close to the classical turning point of the orbit of the Rydberg electron, the electron's velocity is small so that energy transfers $\sim 1\%$ kT are allowed.

In a collision with a molecule there are in addition to the translational energy exchange the possibilities of the molecule gaining or losing rotational energy and losing vibrational energy. The availability of these processes makes inelastic collisions much more likely. Furthermore, both these cases should exhibit resonance phenomena in that after the collision the molecule must be in a specific rotational-vibrational state. How apparent such resonance phenomena are is influenced by several factors.

Let us first consider collisions of Rydberg atoms with ground-state atoms. A well studied process is the collisional angular momentum mixing of nearly degenerate l states of the same n. Excellent examples are the Na nd states and Rb nf states which have quantum defects of ~ 0.01 and are thus nearly degenerate with the higher l states of the same n. For example the Na 10d state is 2 cm^{-1} below the $n = 10$, $l > 2$ states (1% kT). Both the Na nd states and Rb nf states can be selectively excited by laser techniques and as a result collisional angular momentum mixing has been studied in some detail. Experimentally it is observed that an initially populated Na nd or *Rb* nf state is rapidly depopulated by collisions with, for example, rare gas atoms, and this population is transferred to the higher l, m states of the same n (Gallagher *et al* 1977*b*, Hugon *et al* 1979). Collisions continually redistribute the population over all the l, m states with the result that the collisional mixture decays at a rate scaling as $n^{4.5}$, as expected for radiative decay of a mixture of all l, m states (Bethe and Salpeter 1957).

Large cross sections are observed for this process. For example in figure 12 we show the experimental cross sections for the collisional l-mixing of the Rb nf states by He, Ar and Xe (Hugon et al 1979) and the limits for the cross sections obtained using the model of de Prunelé and Pascale (1979). At low values of n the cross sections increase in proportion to the geometric size of the orbit of the Rydberg electron, but at high n they saturate and eventually decline. The border between low and high n is determined by the electron scattering length of the rare gas. For He, with a small scattering length, it is lower than for Xe, which has a larger scattering length. Thus in figure 12 the Xe, Ar and He data are low n, intermediate n and high n respectively. The origin of this behaviour can be understood from the binary encounter model. Recall first our physical picture of the collision; a He atom passes through the Rydberg atom and the Rydberg electron scatters from it nearly elastically, only changing its direction. This corresponds to changing the l and m of the electron. The short-range electron–He interaction between initial and final states $\langle \mathrm{i}|$ and $|\mathrm{f}\rangle$ may be represented by the matrix element

$$\langle \mathrm{i}|V|\mathrm{f}\rangle = \langle \mathrm{i}|2\pi a\delta(\boldsymbol{r}-\boldsymbol{R})|\mathrm{f}\rangle \tag{5.2}$$

where a is the electron scattering length for He and $\boldsymbol{r}$ and $\boldsymbol{R}$ are the coordinate vectors of the Rydberg electron and the He atom relative to the Na^+ core. To obtain the cross section the interaction matrix element must be integrated over the path of the He atom through the Rydberg electron cloud. The n dependence of the cross section thus depends on the scattering length a, the He path length through the Rydberg atom and the density of the electron cloud, as reflected by the normalisation of $\langle \mathrm{i}|$ and $|\mathrm{f}\rangle$. The radius of the Rydberg electron's orbit, and thus the He path length, scales as n^2. Correspondingly the average density of the electron cloud scales as n^{-6}, although the normalisation of $\langle \mathrm{i}|$ and $|\mathrm{f}\rangle$ scales as $n^{-3/2}$. At low n, the Rydberg electron cloud is

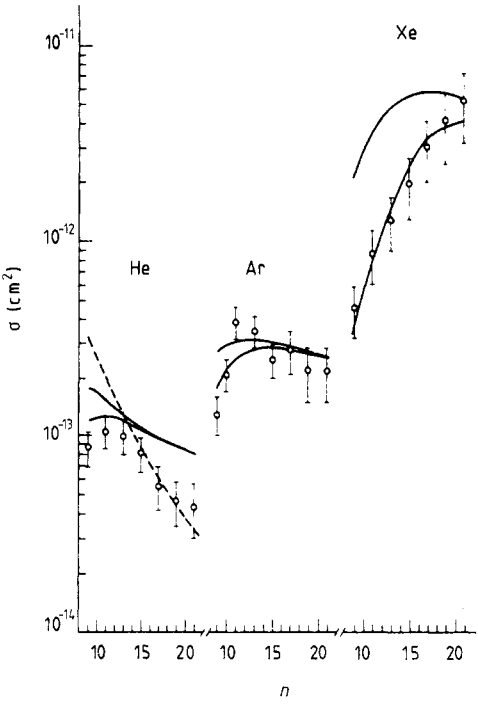

Figure 12. Angular momentum mixing cross sections of Rb (nF) levels for He, Ar, and Xe perturbing atoms, showing the experimental results (○) of Hugon *et al* (1979). Full lines indicate theoretical lower and upper limits for the cross section (de Prunelé and Pascale 1979).

dense enough such that the passage of the He atom anywhere through it induces the Δl transition; thus the cross section increases as the geometric size of the atom. As n is increased the decreasing density of the Rydberg electron cloud reduces the interaction matrix element to the point that the mere presence of the He atom no longer ensures that a state-changing collision will occur, and the cross section reaches a plateau. Finally as n is increased even further, the cross section actually decreases, roughly as n^{-4}, due to the n^{-6} scaling of the electron density and the n^2 dependence of the path length. In fact for $n \approx 40$ the cross section which can be inferred from echo experiments is 40 Å^2 (Flusberg *et al* 1979), roughly comparable to the cross sections expected for Na^+-He interactions (Omont 1977). For a cross section this small, though, it is evident that a binary encounter approach is not meaningful.

Although total collisional l-mixing cross sections can be explained quite well by existing theories, it is possible to explore the process in more detail. For example, how is the mixture of all l and m states produced? Does it happen in one collision with no selection rule or does it occur by a sequence of $\Delta l = \Delta m = 1$ transitions, for example? Calculations show minimal Δl propensity rules, but a definite propensity for small Δm ($\Delta m \leq 2$) in the l-changing collisions (Hickman 1983). Experiments with Na nd states and Xe and Ar collision partners indicate that when ~50% of the atoms have been removed from the initially populated nd states by collisions, most of them are evenly spread over all l states, but with $m < 2$. This is inferred from the fact that the field ionisation signal is what would be expected for the adiabatic ionisation of the $l > 2$, $m \leq 2$ states (Kachru *et al* 1983). In contrast, measurements of Xe nf l-mixing

by Xe in which the adiabatic ($m \leq 2$) field ionisation features are not resolved show diabatic ionisation signals corresponding to models based on the diabatic ionisation of all m states (Slusher *et al* 1982). These two sets of measurements and the calculations seem to infer that what most likely occurs is rapid l mixing followed by slower m mixing.

Another rather interesting aspect of the proposed model for the collision is that the delta function form of the interaction requires that there be good spatial overlap of the initial- and final-state wavefunctions. This is generally true for all the spherically symmetric l states, but it is not true for the Stark states in an electric field. In the Stark states the electron is localised on one side of the atom or the other depending upon the Stark shift of the state. Thus there is calculated to be a strong propensity for transitions to neighbouring Stark states, in contrast to the absence of any propensity rule governing the Δl transition in zero field. Unfortunately, in the atoms studied experimentally, Na and Xe (Kachru *et al* 1983, Slusher *et al* 1982), it was necessary to apply large enough fields that not only were the states transformed to Stark states, but they were also split in energy introducing more inelasticity into the collisions. As a result, while the l-mixing cross sections decreased with electric field it is not completely clear whether the decrease should be attributed to the wavefunction deformation or to the increased inelasticity.

As the energy separation between the Rydberg levels is increased, more energy must be transferred to or from the Rydberg electron in the collision, or, the Rydberg electron–atom scattering must become more inelastic. The collisional depopulation of the lower l states, which have large quantum defects, is a good example of this. From our simple expression of (5.1) for the collisional energy transfer from the Rydberg electron to an atom it is clear that the velocity of the Rydberg electron must be higher, and thus the electron–atom collision must occur at a smaller orbital radius, closer to the ion core of the Rydberg atom. This is in fact observed. Experimentally, these cross sections are found to be quite small, rising from <1 Å^2 at $n \sim 5$ to a plateau of 10–100 Å^2 at $n > 10$ (Gallagher and Cooke 1979d, Gounand *et al* 1977). Such small cross sections, while in agreement with the general requirement based on electron–atom scattering, suggest that the binary encounter approximation is probably no longer valid, and that the ion core needs to be considered as well.

In the collisions of Rydberg atoms with ground-state molecules, as opposed to atoms, the greatest differences stem from rotational and vibrational degrees of freedom of the molecule and the possibility of electrostatic couplings between the Rydberg electron and the permanent multipole moments of the molecule (Matsuzawa 1982). However, for nearly elastic processes molecules are similar to atoms. For example for $n \leq 15$ the l mixing of the Na nd states by CO and N_2 is almost identical to that seen with Ar (Gallagher *et al* 1977e). This is of course a nearly elastic process which can occur by a very short range electron–CO or electron–N_2 interaction or an even multipole interaction which can occur with no change in the rotational energy of the molecule. Processes such as dipole excitations of the molecule are not allowed, for it is not energetically possible to change the molecular rotational energy only by an l change of the Rydberg electron. In view of these considerations it is hardly surprising that in elastic processes a small molecule behaves like an atom.

If we now begin to examine more inelastic processes we can see the effects of the rotational degrees of freedom. For a polar molecule, such as NH_3, HB_r, and CO, there is a long-range electron–dipole coupling, and for virtually all molecules there is a quadrupole coupling. In the case of dipole and quadrupole couplings there must be a change in the rotational quantum number J of $\Delta J = \pm 1$ and $\Delta J = 0, \pm 2$ respec-

tively. These ΔJ requirements imply that there are resonances in the energy transferred corresponding to the rotational intervals of the molecule. Although the long-range electron-dipole coupling suggests that such resonances should be readily visible, this is not always the case simply because the thermal molecular population is spread over many rotational states, obscuring the resonances associated with each particular rotational state. However, for light molecules such as NH_3 and HF it has been possible to observe such resonances (Smith *et al* 1978). An example of this is shown in figure 13, a recording of the field ionisation signal from the Xe 23f state after collisions with NH_3. Note that a group of $n > 23$ states is excited corresponding to each $\Delta J = 1$ transition of NH_3.

For a heavier molecule, such as CO, the rotational collisional resonances do not lead to the same well resolved structure of figure 13, due to the unresolved resonances of the many thermally populated rotational states. Nonetheless their importance is undiminished. As shown by Petitjean *et al* (1984), in collisions of Rb Rydberg states

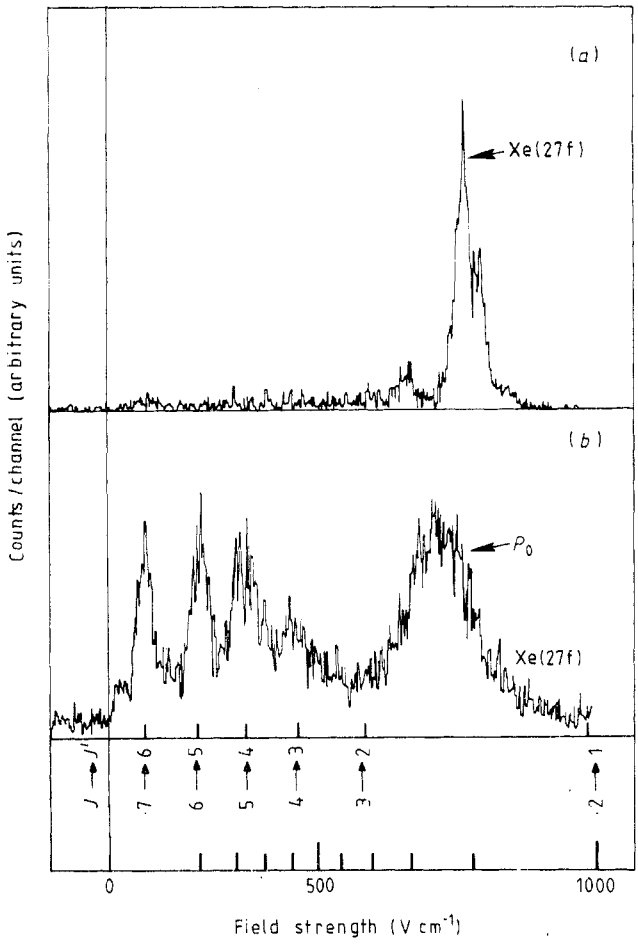

Figure 13. Field ionisation signal from initially excited Xe 27f atoms showing the final-state distribution: (*a*) with no Xe; (*b*) with 10^{-5} Torr NH_3. In (*b*) the final states expected for the $J \rightarrow J'$ rotational transitions are shown. The data clearly show the resonant rotational→ electronic energy transfer (Smith *et al* 1978).

the total depopulation cross section does not show dramatic resonances due to the many thermally populated rotational states, but it is dominated by the inelastic rotational excitation, not by the nearly elastic l-mixing, which has a factor of three smaller cross sections.

The obvious limiting case of the collisional excitation by rotational de-excitation of the molecule is ionisation, and in fact this has been clearly seen for the light hydrogen halide molecules. One of the clearest examples is the ionisation of Xe Rydberg states by rotational de-excitation of HF. A series of steps is observed in collisional ionisation probability of Xe as a function of the Xe binding energy (Matsuzawa and Chupka 1977). The steps occurred at the Xe binding energies corresponding to the $J \rightarrow J-1$ molecular transitions for $J = 1, 2, 3$.

The energy transfer can be to or from the rotation of the molecule, but in the case of vibration it can usually only be to the molecular vibration simply because at thermal energies only the lowest vibrational state is populated in a permanent gas. From our point of view, molecular vibrations can be expected to play a similar role to molecular rotations. In particular, there should be resonances in the inelastic scattering due to the discrete vibrational levels of the molecule. To date only one example of this has been recorded (Gallagher *et al* 1980). In the collisions of Na ns Rydberg atoms with CH_4 and CD_4 the n dependence of the total depopulation cross sections is almost like Xe, rising smoothly from $n = 5$ to $n = 11$. However, there are several anomalously high points: 5s and 6s for CH_4 and 7s for CD_4. Examination of the frequencies of Na transitions with these levels as the upper levels reveals that there are matches with the IR active ν_3 and ν_4 modes of CH_4 and CD_4. Further experimental study indicated that the cross sections for the resonant energy transfers, such as

$$\text{Na } 7\text{s} + CD_4 \rightarrow \text{Na } 5\text{d} + CD_4^*$$

where CD_4^* indicates vibrational excitation of the ν_4 mode, did in fact account for the difference between these three high points and the smooth curves. The large size of these cross sections implies that the interaction must take place nearly at the classical turning point of the lower Na state, and this in turn implies that the cross section for vibrational excitation by electron impact must be quite large at the threshold for vibrational excitation. This has in fact been shown to be the case by low-energy electron scattering from CH_4 (Rohr 1980).

The final collision process which is well described by the binary encounter approach is electron attachment. As an example, consider the process

$$\text{Xe } nf + SF_6 \rightarrow Xe^+ + SF_6^-$$

which is representative of many inert halogen-bearing molecules (West *et al* 1976). The rate constants for electron attachment from Rydberg atoms has been found to be in agreement with the rates predicted from low-energy electron-molecule scattering. Typical cross sections are $\sim 10^4$ Å^2 for $n = 30$ (Dunning and Stebbings 1982).

Collisions between Rydberg atoms and charged particles are dominated by the long-range Coulomb interaction of the charged particle with the entire Rydberg atom. Such behaviour is exhibited by electron and ion collision partners and, in some cases, Rydberg atoms. While not all of the collision processes we shall discuss here have large cross sections it is nonetheless convenient to group them together.

From the point of view of excitation or ionisation, ion and electron collisions are roughly comparable in that it is really only the charge and the velocity of the collision partner which are important. In this connection, the standard velocity for comparison

is the typical velocity, v_e, of the electron in the Rydberg atom, $\sim 1/n$, because when a charged particle is incident with a velocity equal to that of the Rydberg electron, the time average interaction is the strongest, since the orientation of the atomic dipole moment relative to the charged particle is in that case frozen.

First let us consider the case of mixing of nearly degenerate levels by charged particles. In particular the now familiar collisional l mixing of Na nd atoms for $n \sim 25$ by a variety of ions has been studied by crossed ion-atom beam techniques in the velocity-matching region (MacAdam *et al* 1980). There are several very interesting observations which have been made. First, the cross sections are large, $\sim 100\ \pi n^5 a_0^2$, increasing even more rapidly than the geometric cross sections. Second, as expected, there is no dependence on the identity of the ion only on its velocity, i.e. He^+ and Ar^+ at the same velocity produce the same cross section (MacAdam *et al* 1981). Although detailed calculations have been done for such collisions (Percival and Richards 1977) it is possible to understand the size of the cross sections using a simple picture related to our previous discussion of microwave ionisation. As a singly charged ion passes by the Rydberg atom with impact parameter b it produces a maximum field of $1/b^2$ at the Rydberg atom. This field will shift the $l > 2$ states into approximate degeneracy with the d states when

$$\tfrac{3}{2}n^2(1/b^2) = \mu_d/n^3. \tag{5.3}$$

This leads to $b^2 = 3n^5/2\mu_d$ or a cross section equal to $\sim 100\ n^5$ as observed.

As in the case of l mixing by neutral atoms there is the obvious question regarding the distribution of final states and how it is produced. Are there Δl and Δm selection rules? MacAdam *et al* (1985) have clearly shown that there is a very evident evolution of the diabatic field ionisation signal, from $m| > |2$ states, with exposure to the ion beam, showing clearly the existence of a Δm or Δl selection rule. They have compared their results to a hydrogenic model for diabatic ionisation which implies that the final mixture of l, m states is produced by a series of small Δl or Δm steps. They interpret this as being a selection rule for Δl and Δm. On the other hand, Smith *et al* (1983) who analysed the adiabatic $|m| < 2$ field ionisation products of Na nd and K^+ collisions, concluded that after one collision there was an apparent Δm restriction but no Δl selection rule. If in fact the observations of MacAdam *et al* are due mainly to the high-statistical-weight, higher-m states then the pair of measurements seems to argue for a Δm but not a Δl selection rule, just as for l mixing by ground-state atoms.

If we consider collisions in which the ion drives the Rydberg atom to an energetically removed state, $\Delta n \neq 0$, we find that the cross sections are smaller. This occurs for two reasons. First, the transition dipole moments are generally smaller and, second, the energy gaps are larger, requiring more energy exchange with the incident ion. The effect of only one of these changes can be seen in the collisions of Na ns states with ions. In this case there is a substantial energy separation, $0.3\ n^{-3}$, from the nearest state but the dipole matrix elements are still large. Nonetheless the cross sections are at least an order of magnitude smaller than those observed for the nd states for which the energy separation to the high l states is $\sim 0.01\ n^{-3}$ (MacAdam *et al* 1981). An interesting question is whether or not the cross section would be larger for ion collisions with the Na nf states which are separated from the $l > 3$ states by $\sim 0.001\ n^{-3}$.

The logical extension of ion-induced Δn transitions is $\Delta n \to \infty$, or ionisation, and several measurements of this have been made. Measurements of

$$N^{3+} + H^{**} \to H^+ + N^{3+} + e^-$$

for $n = 25$ at high velocities $v/v_e \sim 10$ have shown apparent cross sections which scale

as n^3 (Kim and Meyer 1980), but when the contribution from excitation to levels above $n = 28$, which are field ionised, is taken into account the cross sections exhibit the expected high-velocity n^2 dependence (Olson 1981).

At velocities near velocity matching $v \approx v_e$, the direct ionisation cross section and the charge-exchange cross section become comparable, and both are roughly the geometric size of the Rydberg atom. That the charge-exchange cross section should only become important as the velocity is lowered to velocity matching is hardly a surprise, for in that case the Rydberg electron really has the same velocity relative to its original ion core and to the incident ion and can leave with either. In figure 14 we show the charge-exchange and ionisation cross sections calculated by Monte Carlo methods (Becker and MacKellar 1984). Note that for $v \leqslant v_e$ the total ionisation cross section, charge exchange plus direct ionisation, is roughly the geometric size of the atom, due mainly to charge exchange, but at high velocities it is due to direct ionisation. The agreement of the total ionisation with the geometric cross section for low collision velocities was demonstrated by measurements of ionisation of H $n = 45$ atoms by protons over a centre of mass energy range of 0.3–60 eV (Koch and Bayfield 1975).

Explicit measurements of charge exchange between Na Rydberg atoms and several ions have been carried out in the velocity-matching region (MacAdam and Rolfes

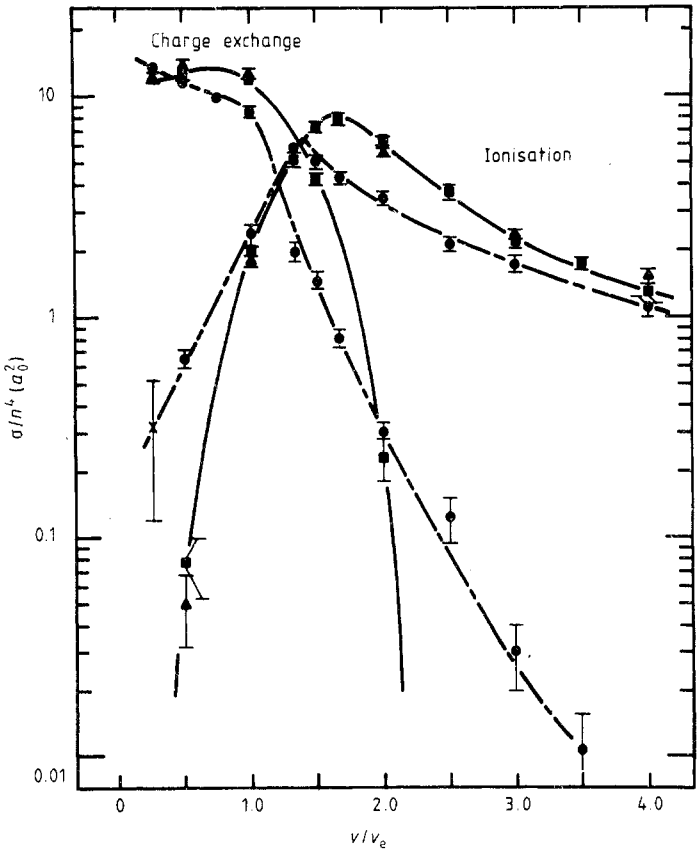

Figure 14. Classical trajectory Monte Carlo ionisation and electron-capture cross sections for $n = 15$, with statistical standard deviations, for specific initial l against reduced velocity: $l = 2$ (●); $l = 14$ (■); $l = 14$ with fixed core (▲) (Becker and MacKellar 1984).

1982, Rolfes and MacAdam 1982). Specifically the final states resulting from the charge exchange between Na Rydberg atoms of $n = 25$-35 and several ions, in particular Na^+, were analysed using field ionisation. Since the charge exchange is expected to have a $\Delta m = 0$ selection rule it was assumed that the field ionisation signals of the Na charge-exchange products could be interpreted assuming adiabatic field ionisation. Making this assumption allows one to assign an n distribution of final states to the observed field ionisation signals. The observed signals are essentially continuous functions of the ionising field strength indicating that there is no strong Δl selection rule, for this would produce readily observable structure. As shown by figure 15, it is peaked near the n of the initial Rydberg state, slightly higher in n for lower incident velocities and slightly lower for higher incident velocities. These results agree with calculations based on the Born approximation and classical Monte Carlo calculations in that the n distribution of the final states is peaked at or near the n of the initial state. However, the width of the observed distributions does not agree particularly well with theoretical predictions.

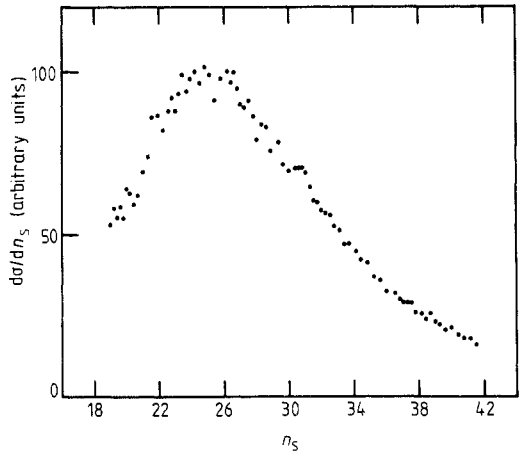

Figure 15. Normalised final-state distributions that result from charge transfer between 750 eV Na^+ and Na in the 24d state plotted against n_S, the effective quantum number in the ionising field (Rolfes and MacAdam 1982).

Thermal electron collisions with Rydberg atoms exhibit much the same behaviour as ion collisions, with the obvious exception of charge exchange. The only systematic measurements which have been carried out are for He Rydberg states excited from the metastable level with a laser in a stationary afterglow (Delpech *et al* 1977, Devos *et al* 1979). The populations of all l states of the same n were monitored by time-resolved $np \rightarrow 2s$ fluorescence to determine the total population and depopulation rates by thermal electrons. An example of this is shown in figure 16 (Devos *et al* 1979), plotting the time-resolved fluorescence from the $n = 9$-15 states after excitation of the $n = 13$ level. From figure 16 and analogous data several conclusions may be drawn. First the collisional mixing of the degenerate lm levels of the same n is immeasurably rapid and is therefore at least two orders of magnitude faster than Δn changing rates. From the build-up times of the fluorescence for $n \neq 13$ levels the cross sections to those levels can be determined, and they are $\sim 10^{-11}$ cm^2. As can be inferred from figure 16 the cross sections decrease rapidly with increasing Δn, and this dependence is in agreement

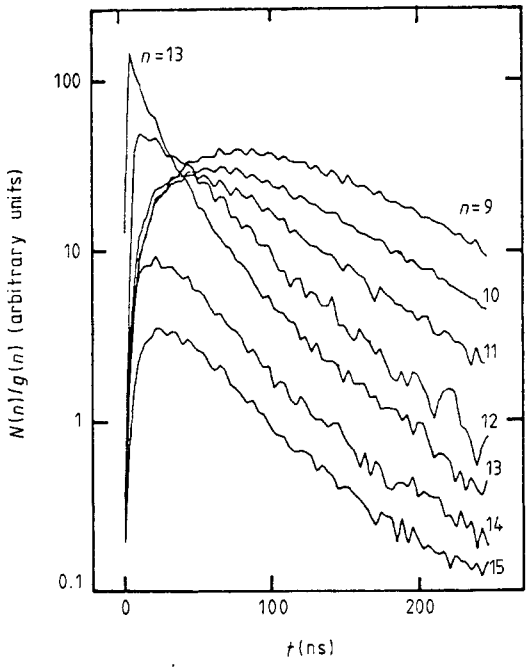

Figure 16. Temporal evolution of the populations divided by the degeneracies $N(n)/g(n)$ of the He $n = 9$-15 levels after selective excitation of the $n = 13$ level by a laser tuned to the 2^3S-13^3P transition at 2645 Å. The electron number density is 2×10^{11} cm^{-3}. The ground-state helium number density is 6.6×10^{16} cm^{-3} and the temperature is 400 K (from Devos *et al* 1979).

with the Monte Carlo calculations of Mansback and Keck (1969), and show clear disagreements with a more analytical approach (Johnson and Hinnov 1969) based on more restrictive assumptions, such as dipole transitions, which predicts a strong $\Delta n = \pm 1$ selection rule.

As we noted above, the collision between two Rydberg atoms is similar to charged particle collisions in that it is still the interaction of a Rydberg atom with two other spatially separated charges. Not unexpectedly if two Rydberg atoms collide they are expected to ionise with a cross section equal to the geometric cross section over a wide range of velocities (Olson 1980, Becker and MacKellar 1979). Note that for any thermal velocity of the atoms the electron velocities are matched, so it is not surprising that the ion collision results would be reproduced.

Two types of Rydberg atom-Rydberg atom collisional effects have been observed. The first is the line broadening in the optical excitation by van der Waals interactions (Raimond *et al* 1981). The second is resonant collisional energy exchange, of the form

$$\text{Na } ns + \text{Na } ns \rightarrow \text{Na } np + \text{Na}(n-1)\text{p}$$

which occurs when the levels are tuned with an electric field so the ns level lies midway between the two np levels so that one ns atom can gain exactly as much energy as the other loses. This process has been observed in the beam-beam scattering of a thermal beam of Na atoms (Safinya *et al* 1981). The collisional resonances observed for the process Na 20s + Na 20s → Na 20p + Na 19p are shown in figure 17. The two striking characteristics of the process are the large size of the cross sections, 10^9 Å^2 at $n = 20$,

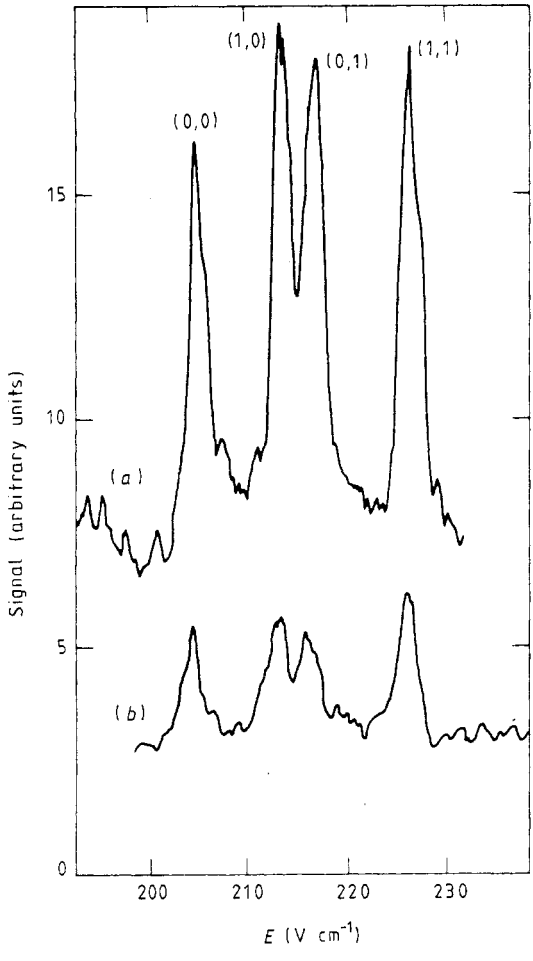

Figure 17. Signal from the Na 20p state, after populating the 20s state, against the static electric field at relative laser powers (*a*) 1.0 and (*b*) 0.4. The background signal, at 250 V cm^{-1} for example, is due to black-body radiative transfer and is linear in laser power; however, the collisional resonances are labelled by the $|m|$ values of the 20p and 19p states, i.e. ($|m|_{20p}$, $|m|_{19p}$) (Safinya *et al* 1981).

and the sharpness of the resonances, ~1 GHz at $n = 20$, corresponding to a collision time of 1 ns. Although these values are at first a little hard to believe, it is straightforward to show that they are to be expected. We recall that this is a resonant dipole-dipole process. We can think of one of the atoms as a dipole μ_1 rotating at its ns-np transition frequency. This rotating dipole produces an oscillating field of magnitude $E_1 \approx \mu_1/r^3$ at the second atom, which is a distance r from the first. If we now imagine the first atom moving past the second with relative velocity v and impact parameter b then the second atom sees a burst of oscillating field from the passing first atom, which can drive its ns$-(n-1)$p transition. For this to occur during the collision requires that

$$\mu_2 E_1 t = 1 \tag{5.4}$$

where μ_2 is the ns-$(n-1)$p transition dipole moment of the second atom, E_1 is the field from the first atom, and t is the collision time. Taking $t = b/v$ and $E \approx \mu_1/b^3$

during the collision time, we find that

$$\sigma = b^2 = \mu_1\mu_2/v \approx n^4/v \tag{5.5}$$

and

$$t = (\mu_1\mu_2/v^3)^{1/2} \approx n^2/v^{3/2}. \tag{5.6}$$

Recalling that thermal velocities are $\sim 10^{-3}$ in atomic units we recover the $n = 20$ values given earlier. The n scalings of the cross sections and collision times given in (5.5) and (5.6) have been verified. In addition, by velocity selecting the beam to produce a lower collision velocity the velocity dependence of the collision time has been verified in a qualitative fashion (Stoneman *et al* 1987a).

These resonant collision processes, while something of a curiosity in themselves, provide interesting research opportunities due to the large dipole moments and long collision times. For example, it has been possible to observe in a quantitative fashion radiatively assisted collisions in which one or more microwave photons are absorbed while the atoms are colliding (Kachru *et al* 1982, Pillet *et al* 1983a). While single photon processes are observable using ground-state atoms and intense (MW) lasers, quantitative multiphoton studies using such an approach are beyond reach. In contrast, using Rydberg atoms and ~ 1 W microwave sources quantitative measurements of collisions in which many photons are emitted or absorbed can be made (Pillet *et al* 1983a). In addition, the long times of the collisions may allow external control of the collision time.

6. Planetary atoms

Thus far we have concentrated on Rydberg atoms which have one electron in a state of high principal quantum number. As we have already pointed out these are hydrogen-like atoms. The behaviour of electrons with two Rydberg electrons has also been considered. The presence of the second electron introduces qualitatively different behaviour. If we choose He as a model we can trace the evolution of such double Rydberg states from the familiar bound states of He. The bound 1snl Rydberg states of He are essentially hydrogenic because all of the excited states of He^+ are so far away that no He states converging to them fall anywhere near the first ionisation limit. If we replace the 1s electron with a 2s electron, we can immediately see two manifestations of the correlations of the two electrons. One of these is autoionisation. The 2snl states are degenerate with 1s $\varepsilon l'$ continua, and the 2snl states autoionise by the Coulomb interaction of the two electrons. This form of electron correlation is common to all multielectron atoms. Peculiar to He is the fact that the 2s and 2p states of He^+ are degenerate, so that the Rydberg series converging to these two limits are roughly degenerate and interact so strongly that labelling the series as 2snl and 2pnl is not useful. This was explicitly shown by the VUV He absorption spectra of Madden and Codling (1963). They observed two series converging to the $n = 2$ state of He^+, one strong and one weak. Cooper *et al* (1963) successfully interpreted the spectra in terms of + and − series which are in essence linear combinations of 2pns and 2snp series. One can think rather heuristically of the + and − series as arising from the Stark splitting of the 2s and 2p states by the Rydberg electron slowly orbiting around the He^+ core. More generally, an atom with two excited electrons, one in a considerably

larger orbit around the ion core than the other, was investigated using classical mechanics by Percival (1977), who termed such atoms planetary atoms because of their similarity to the solar system.

The other method of studying doubly excited states has been by electron scattering, in which the doubly excited states are manifested as resonances in the electron scattering (Schulz 1973). In fact, one of the most illuminating experiments has been carried out by Buckman *et al* (1983), who studied the production of metastable He by electron impact excitation. In their experiments, they observed He^- resonances below the resonances corresponding to excited He states. The most important aspect of their findings is that the series of He^- resonances cannot be fitted with constant quantum defects. For example, the lowest energy resonance associated with each principal quantum number has a quantum defect which increases with energy. This is the clear signature of a sequence of correlated two-electron states, which cannot be described by a constant quantum defect, as can one-electron states.

If we consider the He states $n'l'nl$, where $n' \approx n$, there is no obvious simple picture to describe such atoms. However, there are several theoretical approaches which are described by Fano (1983). One is a normal mode analysis based on the O(4) symmetry of two-electron atoms (Herrick and Kellman 1980, Herrick *et al* 1980). The important regularities disclosed by this approach are progressions of levels with increasing total angular momentum and the grouping of levels into 'supermultiplets' which are very similar to the rotations and vibrations of a triatomic molecule (Ezra and Berry 1982).

The other theoretical approach is based on hyperspherical coordinates (Read 1977, Lin 1983, 1984). If r_1 and r_2 are the radial coordinates of the two electrons then $R = (r_1^2 + r_2^2)$ gives the overall size of the atom and $\alpha = \tan^{-1}(r_1/r_2)$ is introduced to explicitly express the radial correlation. Assuming that the variations in R are slow compared to the variations in α, the motions can be separated much the way electronic and nuclear motions of a molecule are separated in the Born-Oppenheimer approximation. This approach gives reasonably accurate energies for low-lying correlated states of alkaline earth atoms. It has also been used to develop a modified Rydberg formula which accurately predicts the energies of two-electron states (Read 1977).

Potentials as functions of the coordinates R and α may be constructed which are roughly equivalent to molecular potential curves. These potentials have the interesting characteristic that there is a maximum at $\alpha = 45°$, $r_1 = r_2$, which is sometimes called the Wannier ridge. The existence of such a ridge suggests that it is unlikely that many states will be found with the two electrons having similar orbital radii. An implication of this is that excitation just above the double ionisation limit should not produce two low-energy free electrons, but one higher-energy free electron and one electron bound in a Rydberg state of the ion. Electron scattering from He has supported this to some extent. When electrons are scattered from He and low-energy electrons collected, a decrease in signal is observed just above 24.6 eV incident energy, which is the ionisation potential of He (Cvejanovic and Read 1974). As this is the energy at which two low-energy electrons can be formed, one might expect if anything an increase. Thus a decrease seems to imply that the production of two low-energy electrons is unlikely, in agreement with the Wannier ridge prediction of the hyperspherical model.

While electron scattering and synchrotron experiments have the energy range to reach the planetary or double Rydberg levels of any atom and thus have produced most if not all the experimental data to date, they both suffer from relatively poor resolution. Thus much attention has been focused on laser experiments in the hope of cleanly producing such atomic states. The alkaline earth atoms appear to be logical

candidates for two reasons. First, they have two valence electrons and are therefore somewhat He-like. As a result any spectra which are obtained stand a much better chance of being interpreted than the analogous spectra from a more complex atom. Second, the second ionisation limits of the alkaline earth atoms are low. For example, the ground state of Ba^{++} lies only 15 eV above the ground state of Ba. Since present-day tunable laser sources work well at wavelengths down to 2000 Å, or up to photon energies of ~6 eV, the total energy required is not a trivial consideration.

In the alkaline earth atoms it is completely straightforward to excite the bound Rydberg states, such as the Ba 6s*nl* states, using methods exactly like those used to excite the bound states of Na. This provides an ideal starting point for the excitation of the 6p*nl* states, which are autoionising Rydberg states. These states may be excited from the 6s*nl* state by driving the 6s electron to the 6p state with the outer *nl* electron remaining a spectator (Cooke *et al* 1978). As this is in essence the resonance line of Ba^+, the $6snl \rightarrow 6pnl$ transition is much stronger than direct photoionisation, $6snl \rightarrow 6s\varepsilon l+1$, and readily observed. This technique has made it possible to probe many fine details of the Ba autoionising 6p*nl* states and their analogues in other atoms. The interaction between the Ba 6p and *nl* electrons is clearly manifested by the autoionisation of these levels. As a rule the autoionisation rates of the 6p*nl* states scale as ν^{-3} where ν is the effective quantum number of the *nl* state. An example of this, for the Ba 6p*n*d states is shown in figure 18 (Gounand *et al* 1983). With the exception of the $6p_{1/2}nd$ states of $n=16$ the ν^{-3} scaling is quite evident.

The origin of the ν^{-3} scaling is easily understood. Autoionisation occurs by means of the electrostatic coupling between the two electrons which couples the 6p*nl* state to a $6s\varepsilon l'$ continuum, for example. The electrostatic coupling is maximal when the

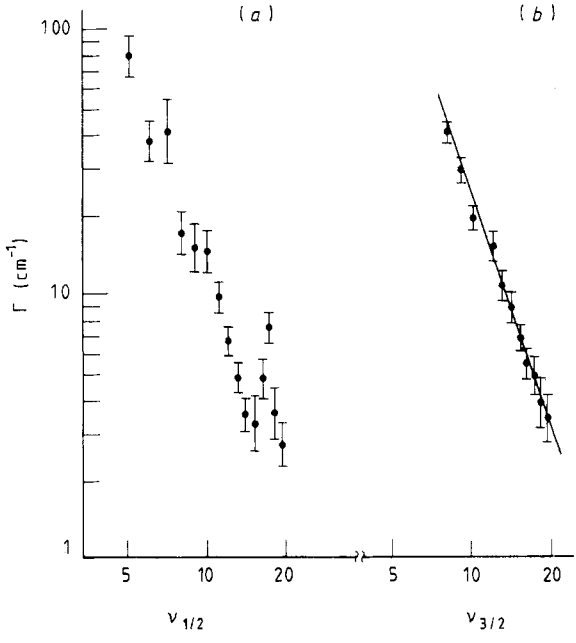

Figure 18. Autoionisation widths Γ of the $J=3$ series for (*a*) Ba $6p_{1/2}nd_{5/2}$ and (*b*) Ba $6p_{3/2}nd_j$. The $6p_{3/2}$ series shows a regular $\nu_{3/2}^{-3}$ variation of the autoionisation rate, but the $6p_{1/2}$ series shows an obvious peturbation at $\nu_{1/2} \sim 16$ due to interaction with the $6p_{3/2}$ series (Gounand *et al* 1983).

two electrons are near each other, and this occurs only when the Rydberg nl electron is near the Ba^+ ion. Thus the autoionisation rate is determined by the normalisation of the Rydberg electron's wavefunction at small radius which scales as $\nu^{-3/2}$. The ν^{-3} scaling can also be thought of in another way. For any given series of l states, the orbital frequency scales as ν^{-3}, so the number of times per second the Rydberg electron passes near the ion core decreases as ν^{-3} (Cooke and Cromer 1985).

While autoionisation is a clear manifestation of the interaction of the two electrons, for the most part the energy levels may be well described as a Rydberg electron added to the Ba^+ 6p state. The mixing seen in the He $2snl$ and $2pnl'$ levels does not occur generally in other atoms because the ion states of different l have different quantum defects. As a result the autoionising states of heavier atoms are actually easier to understand than the autoionising states of He. In figure 18 we have already seen the only complication, which is due to interseries interaction. In Ba, the $6p_{1/2}$ and $6p_{3/2}$ levels of the ion are split by fine structure, and the interaction between series converging to these two fine structure limits alters the regularity of the energy levels and autoionisation rates. The increase of the $6p_{1/2}nd_{5/2}$ autoionisation rate above the ν^{-3} dependence at $n = 16$ shown in figure 18 is due to the interaction with the degenerate $6p_{3/2}$ 10d state which autoionises at an appreciably faster rate. To date, all phenomena associated with low-lying autoionising states can be well explained using multichannel quantum defect theory in which all the two-electron interactions are restricted to a small volume near the ion core. In essence the two-electron effects are introduced as minor perturbations to an independent-electron model.

The ease with which the low-lying autoionising states may be excited by laser techniques encourages the extension of the techniques to excite $n'l'nl$ states where $n' \sim n$. The experimental approach employed has been two-photon excitation from bound $6snl$ states to $n'l'nl$ states. Using several variations of this approach it has been possible to observe higher-lying Ba $n'lnl$ states (Jopson *et al* 1983, Gallagher *et al* 1983, Camus *et al* 1984). A systematic study of Ba $msns$ and $msnd$ states with $m < n$ has been carried out which shows several interesting phenomena (Bloomfield *et al* 1984). First the quantum defects of either series increase by 0.3 with each successive value of m. This is not too surprising, for the Ba^+ core grows progressively larger with m. On the other hand the $msns$ states exhibit a scaled autoionisation rate, the autoionisation rate multiplied by $(\nu)^{+3}$, which is constant as a function of m, while the $msnd$ states exhibit a scaled rate which slowly increases with m. This is shown in figure 19. The difference in the scaled rates can be explained as follows. The autoionisation rates are determined by the interaction between the ms and nl electrons, which occurs mainly at small orbital radius. For the nd states the nl electron is excluded by the centrifugal barrier from very small orbital radius, so increasing the orbital radius of the inner ms electron increases the overlap. On the other hand, the ms states overlap with ns states for all values of m as there is no centrifugal barrier.

One of the most interesting aspects of this work is the fact that even for $n - m = 2$ there is no apparent departure from the model which works for the $6pnl$ states, an outer nl electron attached to a well defined ion core. The $msnl$ states up to $m = 11$ were reached, and states with n as low as $m + 2$ were reached. These limitations are mostly due to the fact that the desired two-photon excitation becomes weaker relative to the single-photon excitation of the continuum, and the latter process eventually obscures the two-photon process of interest. Nevertheless, variations of the two-photon method to avoid this problem have been developed, and there are efforts under way to extend these observations to higher states closer to the Ba^{2+} limit, for

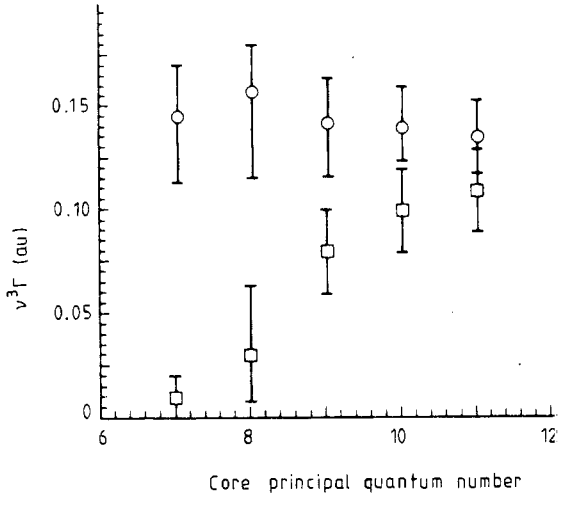

Figure 19. Scaled autoionisation rates, $\nu^3\Gamma$ of the Ba $msns$ (○) and $msnd$ (□) autoionising states (Bloomfield *et al* 1984).

example the 27d45d states have been observed (Boulmer *et al* 1987a). Similarly it is possible to look for strong correlation in the states converging to the degenerate high-l states of Ba^+. These states are quite analogous to the He states and should exhibit the same general structure. In any case it is reasonable to expect the observation of highly correlated atomic states by high-resolution laser techniques in the not too distant future.

7. Experimental techniques

The widespread interest in Rydberg states of alkali and alkaline earth atoms is due in part to the ease with which they may be produced with tunable dye lasers (Hansch 1972). As the ionisation potentials of these atoms range from 4–8 eV, a single visible photon is never energetic enough to populate a Rydberg state so other methods must be used. The simplest of these is to use stepwise excitation through a real intermediate state with two visible lasers. Typical examples are:

$$\text{Ba} \qquad 6s^2 \rightarrow 6s6p \rightarrow \begin{matrix} 6sns \\ 6snd \end{matrix}$$

$$\text{Na} \qquad 3s \rightarrow 3p \rightarrow \begin{matrix} ns \\ nd \end{matrix}.$$

In some cases, such as Cs or Rb, it is easier to frequency double a visible laser to produce the ultraviolet light to excite the high-lying np states. Finally, two-photon excitation through a virtual intermediate state may be used to excite Rydberg states of the same parity as the ground state. While this method has not been used to create large populations in Rydberg states, it is an excellent spectroscopic tool and has led to improved values of the ionisation potentials of several atoms. The most common

of these approaches is the simplest, i.e. stepwise excitation with a pulsed dye laser. Even with a very modest laser of 100 μJ pulse energy and 1 cm^{-1} linewidth it is possible to produce adequate numbers of Rydberg atoms and resolve states up to $n = 60$.

Although laser excitation is the most commonly used approach, not all atoms can be excited from the ground state by a laser, and to study these atoms collisional excitation must be used. The cleanest method is to use electron-impact ionisation, typically by a well defined beam of electrons. This method was used by MacAdam and Wing (1975) to produce He Rydberg atoms for microwave resonance experiments. It has also been used by Kocher and Smith (1977) to produce Rydberg states of Li, and by Freund (1971) to produce Rydberg molecules. Fast beams of hydrogen Rydberg states have been produced by Bayfield and Koch (1974) for microwave ionisation experiments using charge exchange of protons with a gas target.

All of these collision schemes have the attraction of working with any atom or molecule, but they have the disadvantage that an unknown distribution of states is excited. First, it is evident that some range of n and l states will be initially excited, with a production cross section that must fall off as n^{-3}. Second, it is quite possible that subsequent collisions can redistribute the population among the many nearly degenerate Rydberg states. This is not a negligible consideration as the cross sections for state changing by charged particle collisions are substantially larger than the cross sections for the excitation of the Rydberg states.

To circumvent the obvious drawbacks of purely collisional excitation, most experiments with atoms which cannot be excited from the ground state with a laser are now done using a combination of collisional and laser excitation. In general the collision is used to populate a state energetically inaccessible with a laser, and the laser subsequently excites atoms in that state, usually metastable, to a selected Rydberg state. For example, Xe Rydberg states are produced by first exciting a beam of Xe atoms by electron impact, allowing some fraction to accumulate in the metastable state, and then exciting the metastable atoms to Rydberg nf states downstream (Stebbings *et al* 1975). Similarly the utility of fast-beam charge exchange has been greatly improved by adding a 10 μm CO_2 laser which allows the Rydberg states of H and He to be excited from the $n = 10$ levels (Bayfield *et al* 1977, Mariani *et al* 1983). The combination of the line tuning of the CO_2 laser, in 1.8 cm^{-1} steps, and the Doppler tuning which is possible with the fast beam provides a broad tuning range. This first allows the larger population in the $n = 10$ level to be used but, more importantly, allows well defined Rydberg states to be populated.

Rydberg atoms may be detected in several ways, with varying degrees of selectivity and sensitivity. However, all the methods have in common the fact that each Rydberg atom leads to the production of an energetic photon or an ion, either of which can be readily detected. The simplest approach to the detection of a Rydberg state is to detect the fluorescence emitted in the decay of that state. This provides a simple monitor whose intensity is proportional to the number of atoms in the Rydberg state. The wavelength of the fluorescence determines which Rydberg state is being monitored and, depending upon the experiment, anything from a simple coloured glass filter to a monochromator is required. There are several attractions to fluorescence detection. One is the fact that it is well understood, requiring no further interpretation, as does field ionisation. The second is that the photomultiplier can be outside the experimental chamber, allowing easy interchange and adjustment. Finally, in many atoms, but certainly not H, nearly degenerate states of opposite parity can have radically different fluorescent decay wavelengths, and even the crudest coloured filter provides excellent

discrimination. Finally fluorescence is a general technique; it works for all states above the ground state. How well it works is another issue, but in principle it always works.

Fluorescence detection does have some limitations. For instance, it is not very efficient. Quantum efficiencies of photomultipliers are usually in the 1-30% range, but more important, the small solid angle subtended by the photodetector and the losses in the filter or monochromator usually mean overall detection efficiencies of 10^{-4}-10^{-3}. As we have already mentioned, the oscillator strength to the Rydberg states declines as n^{-3}, so for unsaturated excitation, the initial population excited to the Rydberg state by a pulsed laser falls accordingly. As already noted, the lifetimes of the Rydberg states increase as n^{+3}, so the fluorescence intensity scales as n^{-6}, although the time-integrated fluorescence scales as n^{-3}. Due to these considerations, fluorescence detection has been used only up to $n = 22$.

Due mostly to its generality, fluorescence detection has been used in a variety of experiments. In conjunction with pulsed laser excitation it is the obvious way to measure radiative lifetimes, by simply recording the time-resolved exponential decay curves of the fluorescence (Gallagher *et al* 1975). Observing the increase in the fluorescence decay rate with the pressure of a collision partner allows the determination of thermal collision rates in a straightforward way (Hugon *et al* 1979). Finally fluorescence is a natural way to detect quantum beats (Haroche *et al* 1974) in coherently excited states as well as radio frequency transitions between states which fluoresce at different wavelengths (Cooke *et al* 1977).

The detection method peculiar to the study of Rydberg atoms is field ionisation, in which each Rydberg atom is converted into an ion and an electron, both of which can be easily detected. The method is based on the concepts described in a previous section. In its application as a detector an electric field is applied which rises from the near zero field in which the process under investigation occurs to the ionising field in a time short compared to the decay time of the Rydberg state to be detected. In most cases this implies risetimes of $\sim 1\ \mu$s. For the detection of slow-moving thermal beams the rising field is usually produced by the time variation of a voltage pulse. However, the motion of a beam of Rydberg atoms through a spatially varying field has also been used quite successfully (MacAdam and Rolfes 1982). It is particularly useful for fast beams and for continuous-wave (as opposed to pulsed) experiments.

Although most field ionisation detection is done with static, or nearly so, fields this approach will clearly not work to detect the Rydberg states of an ion due to the deflection of the ion. However, a high-frequency field does not produce a net deflection of an ion, and thus microwave ionisation is the logical way to detect Rydberg states of ions, as has recently been shown in the detection of Ba^+ nd Rydberg states (Boulmer *et al* 1986).

The attractions of field ionisation are several. First, it is nearly 100% efficient. Each Rydberg atom is converted to an ion and an electron, all the ions or electrons can be collected by a particle multiplier and the quantum efficiencies for ions and electrons are >50% and 100% respectively. Second, it can be surprisingly selective. If a pulsed field is applied to ionise the atoms, as the ionising field rises, atoms in different states ionise at different times and therefore reach the particle multiplier at different times. Thus it is possible to observe the spectrum of Rydberg states present in the time dependence of the field ionisation signal.

Although field ionisation is a very attractive detection scheme it does have several limitations. The foremost of these is the fact that the response of an atom to a pulsed field depends on the details of the passage from zero field to the high ionising field.

Thus the selectivity varies from one atom to the next and depends in a critical way on the risetime of the ionising pulse. Also the range of n states that may usefully be studied is limited by the n^{-4} scaling of the requisite ionising field. This has limited field ionisation to states of $n \geq 8$, which requires a field of $\sim 10^5$ V cm^{-1}.

Field ionisation detection has found many applications. Radiative lifetimes can be determined by measuring the number of surviving atoms as a function of the delay between pulsed excitation and ionisation. As for fluorescence, the change in the decay rate with increased density of collision partners can be used to determine collision rates (Kachru *et al* 1983). However, unlike fluorescence detection, all nl product states may be observed using field ionisation detection, whereas only the low-l states may be observed with fluorescence detection. This ability has been used to determine final-state product distributions of collision processes (Slusher *et al* 1982). The selectivity of field ionisation has been used frequently in radio frequency resonance measurements (Gallagher *et al* 1977d, Fabre *et al* 1977). The fact that the field ionisation pulse is applied at a controllable time after the excitation allows further flexibility. The obvious application is to detect the quantum beats between coherently excited states. This was originally done with a very fast ionising pulse (Leuchs and Walther 1979), and later with a fast 'freezing' pulse which was followed by a conventional, slow field ionisation pulse (Jeys *et al* 1981).

Collisional ionisation is quite commonly used, especially in laser spectroscopy experiments in which little or no selectivity is required. The collision partners may be nearly anything. The most benign and easy to use are perhaps molecules such as SF_6 which readily attach an electron from a Rydberg atom (Dunning and Stebbings 1982). As the rate constants are quite large, 10^9 cm^3 s^{-1}, low pressures, 10^{-6} Torr, of SF_6 are quite adequate. In this connection it is interesting to note that Rydberg atoms have possible utility as a source of negative ions (Hill 1977). The most common collisional detection scheme is the space-charge-limited diode, or Kingdon cage (Curry *et al* 1976), in which a high density of the atom under study is used. In its simplest form the diode consists of a wire cathode with a coaxial cylindrical anode around it, biased at ~ 1 V positive with respect to the cathode. The wire is heated to produce electrons which produce a space-charge cloud of electrons around the cathode, severely limiting the electron current. The volume inside the anode is filled with the atoms of interest, and when one of them is excited to a Rydberg state it is collisionally ionised, presumably by the thermal electrons, and the resulting ion drifts toward the cathode. As it does so it locally neutralises the space charge of the electrons allowing a local increase in the electron current. Since the ion moves rather slowly compared to an electron many extra electrons, $\sim 10^6$, can escape through the neutralised region as the ion drifts to the cathode. Thus this approach has the same gain as many electron multipliers.

One of the interesting aspects of Rydberg atoms is the ease with which they can be manipulated. An excellent example of this is the Stark switching technique which can be used to populate almost arbitrary l states, bypassing the normal $\Delta l = 1$ optical selection rule (Freeman and Kleppner 1976, Cooke *et al* 1978). In an electric field all Stark states may be optically excited, and if only one is excited, and the field turned off adiabatically, the Stark state returns to a single zero-field l state. Which l state it returns to is determined completely by the energy ordering of the l states and the Stark states. The lowest-energy Stark state of manifold goes adiabatically into the lowest-energy l state, etc. No crossing of the levels occurs. The limitation stems from the requirement that the passage from high to zero field be adiabatic. In practice this probably means that the highest l states, which are nearly degenerate, ~ 10 MHz apart

at $n = 15$–20, cannot be made selectively; nonetheless Sr $5snl$ Rydberg states of l up to 7 have been made in this way (Cooke *et al* 1978). At the opposite extreme, if the field direction is reversed rapidly enough, a completely diabatic passage through zero field occurs with the result that the red state of the manifold becomes the blue state and vice versa (Rolfes *et al* 1983). Both these schemes allow us to modify the l selection rules to produce states of high l, but do not alter the m selection rules. To produce states of high l and m, the 'circular' states, a different approach has been employed which is based on adiabatic rapid passage (Hulet and Kleppner 1983). Using this approach they have succeeded in producing the circular states of Cs.

Having outlined the main production and detection approaches, it is useful to describe, as typical experiments, measurement of ns–np radio frequency intervals (Fabre *et al* 1978) and collision cross sections in Na using pulsed laser excitation and field ionisation detection. These experiments are chosen because they are representative and show how the same basic techniques can be employed to measure quite different properties.

A pulsed Nd:YAG pump laser operating at ~10 Hz is used to pump two tunable dye lasers of ~100 μJ pulse energy, 5 ns pulse width, and 1 cm^{-1} linewidth. These lasers are tuned to drive the Na $3s \rightarrow 3p$ and $3p \rightarrow ns$ transitions. The atomic beam apparatus is a vacuum chamber ~0.5 m in diameter which is held at a pressure of $\sim 10^{-6}$ Torr. The Na atoms effuse from a heated oven and are collimated before passing midway between a pair of field plates, where they are excited by the lasers as shown by figure 20. The intersection of the laser beams and the atomic beam is typically 10 cm from the oven. The collimation is only to keep the Na from coating the field plates. The field plates are 1 cm apart and the upper one has either a hole or a grid to allow the extraction of ions produced by field ionisation of the Na. Typically a voltage pulse is applied to the lower field plate to ionise the atoms and accelerate the ions to the particle multiplier mounted above the field plates. Discrete dynode multipliers or microchannel plates are preferable since they can handle large signals without saturation, and, by the same reasoning, channeltrons are less desirable. The signal from the particle multiplier goes to a gated detector. The microwaves are introduced

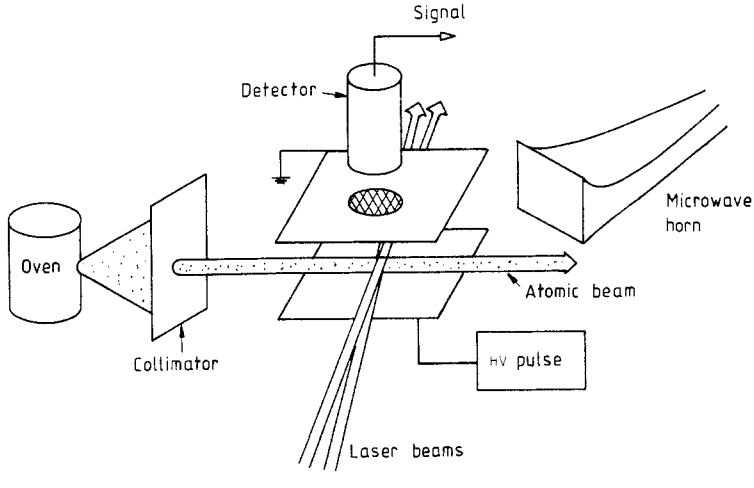

Figure 20. Schematic diagram of an atomic beam apparatus configured to perform microwave resonance spectroscopy. The vacuum vessel and the lasers are not shown explicitly.

by a microwave horn as shown. Each time the laser fires, a population of ns atoms is created. For $\sim 1\ \mu$s after the laser fires the atoms are exposed to the microwave field, and if its frequency is at the ns-np resonance the atoms make the $ns \rightarrow np$ transition. At the time 2 μs after the laser excitation the field ionisation pulse is applied. To detect the ns-np resonance, the field ionisation pulse amplitude must be set high enough to ionise the np state but not high enough to ionise the ns state. Thus a signal is only observed if the microwaves drive the $ns \rightarrow np$ transition. The microwave frequency is slowly (in a matter of minutes) scanned across the resonance, and the np field ionisation signal from many pulses of the laser builds up a resonance curve.

To measure collisional angular momentum mixing of the Na nd states with the higher l states by Xe the same basic apparatus can be used, but the microwave horn must be replaced with a Xe inlet which floods the chamber with Xe at pressures of up to 10^{-4} Torr (Kachru *et al* 1983). There are several approaches to this experiment. One approach is to measure the nd state decay rate as a function of Xe pressure. The decay rate is obtained by monitoring the nd field ionisation signal as a function of the delay time between laser excitation and the field ionisation pulse. The increase in decay rate with Xe pressure gives the depopulation cross section, which is dominated by mixing with states of the same n but $l > 2$. Alternatively it is possible to monitor the increase in field ionisation signal from the $l > 2$ states as the Xe pressure and exposure times are increased.

That the $l > 2$ states are the final states of the collision can be verified by varying the ionising field at a fixed time after the laser pulse when a substantial amount of collisional depopulation of the originally populated nd state has occurred. The dependence of the signal on the amplitude of the field ionisation pulse can be used to infer the final states of the collisions.

Both experiments described here are relatively straightforward ways of approaching the respective problems and they can be refined in many ways. However, the most important point to note is that the method and apparatus used to investigate seemingly different problems are very much the same.

8. Conclusion

The past ten years has been an interesting period in the study of Rydberg atoms. The development of the tunable dye laser (Hansch 1972) made it possible to excite these curious atoms with relative ease, and the immediately subsequent period of research was fueled to some extent by the fascination of these huge weakly bound atoms. Not only were the properties of the atoms themselves new, but also the techniques used to study them. For example, prior to the study of Rydberg atoms, no one would have imagined that field ionisation would be routinely used as a detection method, as it is today. During this period it seemed as though there were many interesting or at least unknown directions to explore, and most of them were explored, providing a fairly solid basis of our understanding of Rydberg atoms. Now we have come to the point where it is necessary to be more critical in choosing problems for which Rydberg atoms are particularly good systems; however, this is not a very severe constraint for Rydberg atoms with their exaggerated properties. They seem to be excellent systems for the study of atoms in strong electric and magnetic fields, both static and oscillating. Similarly they are the perfect choice for the study of single atoms interacting with

radiation fields. Finally they provide the possibility of unique collision processes such as collisions with low-energy scattering and tunable resonant-energy transfer.

It is hard to imagine that the immediate future will bring a technical development which will have the same impact as the dye laser, so it seems fair to assume that the future will bring further development in the direction of more detailed and precise studies of the types of problems outlined above. The one exception to this is the study of atoms excited to near the second ionisation limit where electron correlation should be prominent. Such atoms will probably be observed by incrementally changing and refining the present-day approaches.

Acknowledgments

It is a pleasure to acknowledge many enlightening discussions with my colleagues both in the Molecular Physics Laboratory of SRI International and the Department of Physics of the University of Virginia. This work has been supported by the National Science Foundation.

References

Amaldi E and Segre E 1934 *Nuovo Cimento* **11** 145
Bailey D S, Hiskes J R and Riviere A C 1965 *Nucl. Fusion* **5** 41
Bates D R and Damgaard A 1949 *Phil. Trans. R. Soc.* **242** 101
Bayfield J E, Gardner L D and Koch P M 1977 *Phys. Rev. Lett.* **39** 76
Bayfield J E and Koch P M 1974 *Phys. Rev. Lett.* **33** 258
Becker R L and MacKellar A D 1979 *J. Phys. B: At. Mol. Phys.* **12** L345
—— 1984 *J. Phys. B: At. Mol. Phys.* **17** 3923
Beiting E J, Hildebrandt G F, Kellert F G, Foltz G W, Smith K A, Dunning F B and Stebbings R F 1979 *J. Chem. Phys.* **70** 3551
Bethe H A and Salpeter E E 1957 *Quantum Mechanics of One and Two Electron Atoms* (New York: Academic)
Bhatti S A, Cromer C L and Cooke W E 1981 *Phys. Rev.* A **24** 161
Bloomfield L A, Freeman R R, Cooke W E and Boker J 1984 *Phys. Rev. Lett.* **53** 2234
Boulmer J, Camus P, Gagne M and Pillet P 1987a *J. Phys. B: At. Mol. Phys.* **20** L143
Boulmer J, Camus P and Pillet P 1987b *J. Opt. Soc. Am.* B **4** 805
Buckman S J, Hammond P, Read F H and King G C 1983 *J. Phys. B: At. Mol. Phys.* **16** 4039
Camus P, Pillet P and Boulmer J 1984 *J. Phys. B: At. Mol. Phys.* **18** L481
Chang E S 1985 *Phys. Rev.* A **31** 495
Cooke W E and Cromer C L 1985 *Phys. Rev.* A **32** 2725
Cooke W E and Gallagher T F 1978 *Phys. Rev.* A **17** 1226
—— 1980 *Phys. Rev.* A **21** 588
Cooke W E, Gallagher T F, Edelstein S A and Hill R M 1978 *Phys. Rev. Lett.* **40** 178
Cooke W E, Gallagher T F, Hill R M and Edelstein S A 1977 *Phys. Rev.* A **16** 1141
Cooper J W, Fano U and Prats F 1963 *Phys. Rev. Lett.* **10** 518
Curry S M, Collins C B, Mirza M Y, Popescu D and Popescu I 1976 *Opt. Commun.* **16** 251
Cvejanovic S and Read F H 1974 *J. Phys. B: At. Mol. Phys.* **7** 1841
Delpech J-F, Boulmer J and Devos F 1977 *Phys. Rev. Lett.* **39** 1400
de Prunelé E and Pascale J 1979 *J. Phys. B: At. Mol. Phys.* **12** 2511
Devos F, Boulmer J and Delpech J-F 1979 *J. Physique* **40** 215
Dubau J S and Volonté S 1980 *Rep. Prog. Phys.* **43** 199
Ducas T W, Spencer W P, Vaidyanathan G, Hamilton W H and Kleppner D 1979 *Appl. Phys. Lett.* **35** 382
Dunning F B and Stebbings R F 1982 *Rydberg States of Atoms and Molecules* ed R F Stebbings and F B Dunning (Cambridge: Cambridge University Press) p 315
Ezra G S and Berry R S 1982 *Phys. Rev.* A **25** 1513
Fabre C M, Goy P and Haroche S 1977 *J. Phys. B: At. Mol. Phys.* **10** L183
Fabre C M, Gross M and Haroche S 1975 *Opt. Commun.* **13** 393

Fabre C, Haroche S and Goy D 1978 *Phys. Rev.* A **18** 299
Fano U 1970 *Phys. Rev.* A **2** 353
—— 1983 *Rep. Prog. Phys.* **46** 97
Farley J and Gupta R 1977 *Phys. Rev.* A **15** 1952
Fermi E 1934 *Nuovo Cimento* **11** 157
Figger H, Leuchs G, Straubinger R and Walther H 1980 *Opt. Commun.* **33** 57
Flannery M R 1982 *Rydberg States of Atoms and Molecules* ed R F Stebbings and F B Dunning (Cambridge: Cambridge University Press) p 393
Flusberg A, Kachru R, Mossberg T and Hartmann S R 1979 *Phys. Rev.* A **19** 1607
Fredriksson K, Lundberg H and Svanberg S 1980 *Phys. Rev.* A **21** 241
Freeman R R and Kleppner D 1976 *Phys. Rev.* A **14** 1614
Freund R S 1971 *J. Chem. Phys.* **54** 3125
Gallagher T F 1982 *Rydberg States of Atoms and Molecules* ed R F Stebbings and F B Dunning (Cambridge: Cambridge University Press) p 165
Gallagher T F and Cooke W E 1978 *Phys. Rev.* A **18** 2510
—— 1979a *Phys. Rev.* A **19** 694
—— 1979b *Phys. Rev. Lett.* **42** 835
—— 1979c *Appl. Phys. Lett.* **34** 369
—— 1979d *Phys. Rev.* A **19** 2161
Gallagher T F, Cooke W E, Edelstein S A and Hill R M 1977a *Phys. Rev.* A **16** 273
Gallagher T F, Edelstein S A and Hill R M 1975 *Phys. Rev.* A **11** 1504
—— 1977b *Phys. Rev.* A **15** 1945
Gallagher T F, Hill R M and Edelstein S A 1976 *Phys. Rev.* A **13** 1448
Gallagher T F, Humphrey L M, Cooke W E, Hill R M and Edelstein S E 1977c *Phys. Rev.* A **16** 1098
Gallagher T F, Humphrey L M, Hill R M, Cooke W E and Edelstein S A 1977d *Phys. Rev.* A **15** 1937
Gallagher T F, Kachru R and Tran N H 1982 *Phys. Rev.* A **26** 2611
Gallagher T F, Kachru R, Tran N H and van Linden van den Heuvell H B 1983 *Phys. Rev. Lett.* **51** 1753
Gallagher T F, Olson R E, Cooke W E, Edelstein S A and Hill R M 1977e *Phys. Rev.* A **16** 441
Gallagher T F, Perry B E, Safinya K A and Sandner W 1981 *Phys. Rev.* A **24** 3249
Gallagher T F, Ruff G A and Safinya K A 1980 *Phys. Rev.* A **22** 843
Gounand F, Fournier P F and Berlande J 1977 *Phys. Rev.* A **15** 2212
Gounand F, Gallagher T F, Sandner W, Safinya K and Kachru R 1983 *Phys. Rev.* A **27** 1925
Gounand F, Hugon M, Fournier P R and Berlande J 1979 *J. Phys. B: At. Mol. Phys.* **12** 547
Goy P, Raimond J M, Gross M and Haroche S 1983 *Phys. Rev. Lett.* **51** 343
Gross M, Goy P, Fabre C, Haroche S and Raimond J M 1979 *Phys. Rev. Lett.* **43** 343
Hansch T W 1972 *Appl. Opt.* **11** 895
Haroche S, Gross M and Silverman M P 1974 *Phys. Rev. Lett.* **33** 1063
Herrick D R and Kellman M E 1980 *Phys. Rev.* A **21** 418
Herrick D R, Kellman M E and Poliak R D 1980 *Phys. Rev.* A **22** 1517
Hickman A P 1983 *Phys. Rev.* A **28** 111–118
Hickman A P, Olson R E and Pascale J 1982 *Rydberg States of Atoms and Molecules* ed R F Stebbings and F B Dunning (Cambridge: Cambridge University Press) p 187
Hill R M 1977 private communication
Höglund B and Metzger P E 1965 *Science* **150** 359
Holberg L and Hall J L 1984 *Phys. Rev. Lett.* **53** 230
Hugon M, Gounand F, Fournier P F and Berlande J 1979 *J. Phys. B: At. Mol. Phys.* **12** 2707
Hulet R G, Hilfer E S and Kleppner D 1985 *Phys. Rev. Lett.* **55** 2137
Hulet R G and Kleppner D 1983 *Phys. Rev. Lett.* **51** 1430
Itano W M, Lewis L L and Wineland D J 1982 *Phys. Rev.* A **25** 1233
Jenkins F A and Segre E 1939 *Phys. Rev.* **55** 52
Jeys T H, Foltz G W, Smith K A, Beiting E J, Kellert F G, Dunning F B and Stebbings R F 1980 *Phys. Rev. Lett.* **44** 390
Jeys T H, Smith K A, Dunning F B and Stebbings R F 1981 *Phys. Rev.* A **23** 3065
Johnson L C and Hinnov E 1969 *Phys. Rev.* **181** 143
Jopson R M, Freeman R R, Cooke W E and Bokor J 1983 *Phys. Rev. Lett.* **51** 1640
Kachru R, Gallagher T F, Gounand F, Safinya K A and Sandner W 1983 *Phys. Rev.* A **27** 795
Kachru R, Tran N H and Gallagher T F 1982 *Phys. Rev. Lett.* **49** 191
Kim J H and Meyer F W 1980 *Phys. Rev. Lett.* **44** 1047
Koch P M and Bayfield J E 1975 *Phys. Rev. Lett.* **34** 448
Kocher C A and Smith A J 1977 *Phys. Rev. Lett.* **39** 1516

Leuchs G and Walther H 1979 *Z. Phys.* A **293** 93
Lin C D 1983 *Phys. Rev. Lett.* **51** 1348
—— 1984 *Phys. Rev.* A **29** 1019
Littman M G, Kash M M, and Kleppner D 1978 *Phys. Rev. Lett.* **41** 103
Littman M G, Zimmerman M L, Ducas T W, Freeman R R and Kleppner D 1976 *Phys. Rev. Lett.* **36** 788
Loudon R 1973 *The Quantum Theory of Light* (Oxford: Oxford University Press)
MacAdam K B, Crosby D A and Rolfes R 1980 *Phys. Rev. Lett.* **44** 980
MacAdam K B and Rolfes R G 1982 *J. Phys. B: At. Mol. Phys.* **15** L243
MacAdam K B, Rolfes R and Crosby D A 1981 *Phys. Rev.* A **24** 1286
MacAdam K B, Smith D B and Rolfes R G 1985 *J. Phys. B: At. Mol. Phys.* **18** 441
MacAdam K B and Wing W H 1975 *Phys. Rev.* A **12** 1464
Madden R P and Codling K 1963 *Phys. Rev. Lett.* **10** 516
Mansbach P and Keck J C 1969 *Phys. Rev.* **181** 275
Mariani D R, van de Water W, Koch P M and Bergeman T 1983 *Phys. Rev. Lett.* **50** 1261
Matsuzawa M 1982 *Rydberg States of Atoms and Molecules* ed R F Stebbings and F B Dunning (Cambridge: Cambridge University Press) p 267
Matsuzawa M and Chupka W A 1977 *Chem. Phys. Lett.* **50** 373
Mayer J E and Mayer M G 1933 *Phys. Rev.* **43** 605
Meschede D, Walther H and Muller G 1985 *Phys. Rev. Lett.* **54** 551
Moore C E 1947 *Atomic Energy Levels, NBS Circular no 467* (Washington DC: US Govt Printing Office)
Olson R E 1979 *Phys. Rev. Lett.* **43** 126
—— 1981 *Phys. Rev.* A **23** 3338
Omont A 1977 *J. Physique* **38** 1343
Park D 1960 *Z. Phys.* **159** 155
Percival I C 1977 *Proc. R. Soc.* A **353** 289
Percival I C and Richards D 1977 *J. Phys. B: At. Mol. Phys.* **10** 1497
Petitjean L, Gounand F and Fournier P R 1984 *Phys. Rev.* A **30** 71
Pillet P 1986 private communication
Pillet P, Kachru R, Tran N H, Smith W W and Gallagher T F 1983a *Phys. Rev. Lett.* **50** 1763
Pillet P, Smith W W, Kachru R, Tran N H and Gallagher T F 1983b *Phys. Rev. Lett.* **50** 1042
Pillet P, van Linden van den Heuvell H B, Smith W W, Kachru R, Tran N H and Gallagher T F 1984 *Phys. Rev.* A **30** 280
Raimond J M, Vitrant G and Haroche S 1981 *J. Phys. B: At. Mol. Phys.* **14** L655
Read F H 1977 *J. Phys. B: At. Mol. Phys.* **10** 449
Rohr K 1980 *J. Phys. B: At. Mol. Phys.* **13** 4897
Rolfes R G and MacAdam K B 1982 *J. Phys. B: At. Mol. Phys.* **15** 4591
Rolfes R G, Smith D B and MacAdam K B 1983 *J. Phys. B: At. Mol. Phys.* **16** L533
Safinya K A, Delpech J-F, Gounand F, Sandner W and Gallagher T F 1981 *Phys. Rev. Lett.* **47** 405
Schulz G J 1973 *Rev. Mod. Phys.* **45** 378
Seaton M J 1983 *Rep. Prog. Phys.* **46** 167
Slusher M P, Higgs C, Smith K A., Dunning F B and Stebbings R F 1982 *Phys. Rev.* A **26** 1350
Smith K A, Kellert F G, Rundel R D, Dunning F B and Stebbings R F 1978 *Phys. Rev. Lett.* **40** 1362
Smith W W, Pillet P, Kachru R, Tran N H and Gallagher T F 1983 *Proc. 13th Int. Conf. on Physics of Electronic and Atomic Collisions* ed J Eichler (Amsterdam: North-Holland) p 668
Spencer W P 1981 private communication
Spencer W P, Vaidyanathan A G and Kleppner D 1982 *Phys. Rev.* A **25** 380
Stebbings R F, Latimer C J, West W P, Dunning F B and Cook T B 1975 *Phys. Rev.* A **12** 1453
Sternheimer R M, Rodgers J E, Lee T and Das T P 1976 *Phys. Rev.* A **14** 1595
Stoneman R C, Adams M D and Gallagher T F 1987 *Phys. Rev. Lett.* **58** 1324
Stoneman R C and Gallagher T F 1985 *Phys. Rev. Lett.* **55** 2567
Vaidyanathan A G, Spencer W P and Kleppner D 1981 *Phys. Rev. Lett.* **47** 1592
van Leeuwen K A H, v Oppen G, Renwick S, Bowlin J B, Koch P M, Jensen R V, Rath O, Richards D and Leopold J G 1985 *Phys. Rev. Lett.* **55** 2231
van Vleck J H and Whitelaw N G 1933 *Phys. Rev.* **44** 551
West W P, Foltz G W, Dunning F B, Latimer C J and Stebbings R F 1976 *Phys. Rev. Lett.* **36** 854
Zimmerman M L, Littman M G, Kash M M and Kleppner D 1979 *Phys. Rev.* A **20** 2251